the δ-phase. The origin of such a striking behaviour of thermal expansion in the mixed two-phase region is not understood yet. A short discussion about similar "anomalous" thermal expansion in some other superionics is given at the end of this chapter.

5.3.2 Structural behaviour of superionic α-AgCuS

The recently proposed [51] structural model for hexagonal AgCuS was based on the structural model of Cu_2S determined by single-crystal neutron diffraction [91]. Accordingly, the sulphur ions of α-AgCuS adopt a hcp structure (space group $P6_3/mmc$) on the 2(d) site. At 380 K about 75% of all copper are situated in triangular coordination within hcp sulphur layers, partially occupying the 2(b) site, whereas about 25% of the copper and all silver partially occupy a 12(k) site with triangular coordination (see figure 5.16). The cations on the 12(k) site at (x, $2x$, z) with x=0.246(1) and z=0.436(1) at 380 K are slightly displaced from the faces of the triangular surroundings towards the centers of the distorted sulphur tetrahedra (possible variants of such triangular surroundings and tetrahedra can be seen in figure 5.16). The temperature dependences of the parameters of the average structure of α-AgCuS are presented in figure 5.17. A pronounced non-uniformity has been observed in the thermal behaviour of the positional parameters of the cations on the 12(k) site at (x, $2x$, z), where x increases with temperature and z decreases. This leads to a modest shift of the cations towards the centers of the distorted sulphur tetrahedra (see figure 5.16), which correlates well with a significant cation occupancy of the tetrahedral cavities in δ-AgCuS (see next subsection). The isotropic thermal parameters, u_{iso}, and the distribution of mobile cations between the two types of interstitial sites remain insensitive to temperature changes. An identical structural behaviour was reported for hexagonal copper sulfide, Cu_2S [91]. We therefore propose the same mechanism for the cation transport as reported for Cu_2S in [91]: diffusion through the $(\frac{1}{2}, \frac{1}{2}, \frac{1}{2})$ site in $\langle 111 \rangle$ direction is insufficient. The cation conductivity is assumed to be two dimensional and occurs primarily in slabs perpendicular to the c-direction instead.

The trigonal coordination of copper in the distorted hcp structure of sulphur reflects the principal similarity of the hexagonal and the orthorhombic phases. The possibility of a similar coordination of the cations in the disordered conducting structure relative to their

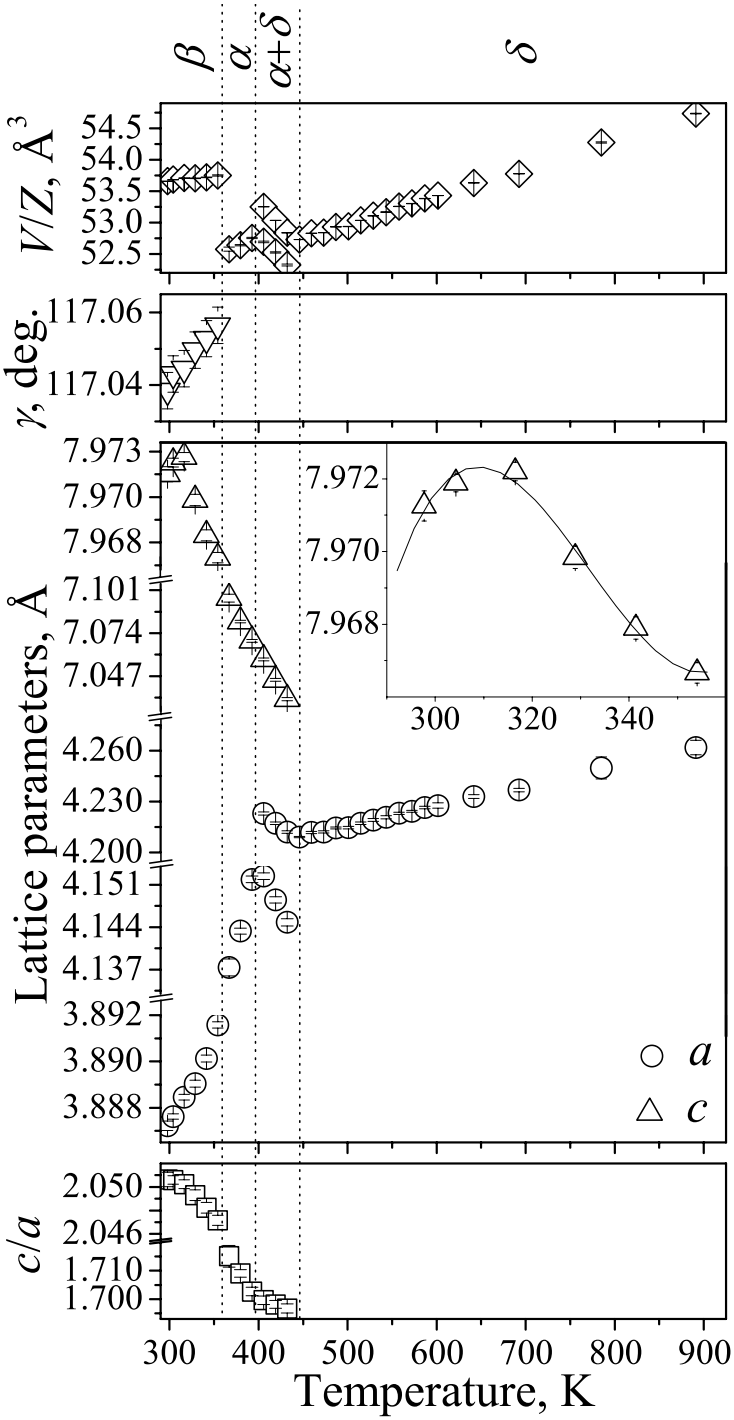

Figure 5.15: The unit cell axial ratio c/a, cell dimensions a, c, γ and unit cell volume per formula unit V/Z of stromeyerite as a function of temperature in the range from RT up to the melting point. The lattice parameters of the primitive pseudo-hexagonal and rhombohedral cells of β- and δ-AgCuS are illustrated. Inset: unusual thermal expansion along c-direction of β-AgCuS.

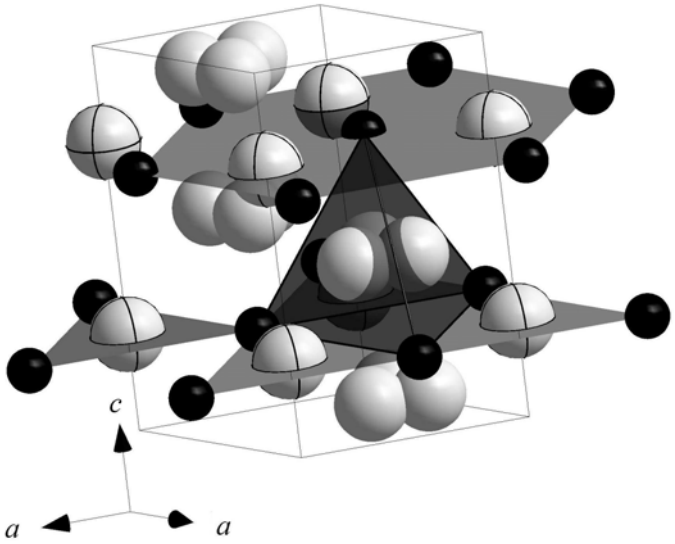

Figure 5.16: A schematic diagram showing the average structure of hexagonal α-AgCuS at 380 K. Black, grey and grey with inner lines spheres are S^{2-} in 2(d), Ag^{+}/Cu^{+} in triangular 12(k) and Cu^{+} in triangular 2(b) sites, respective.

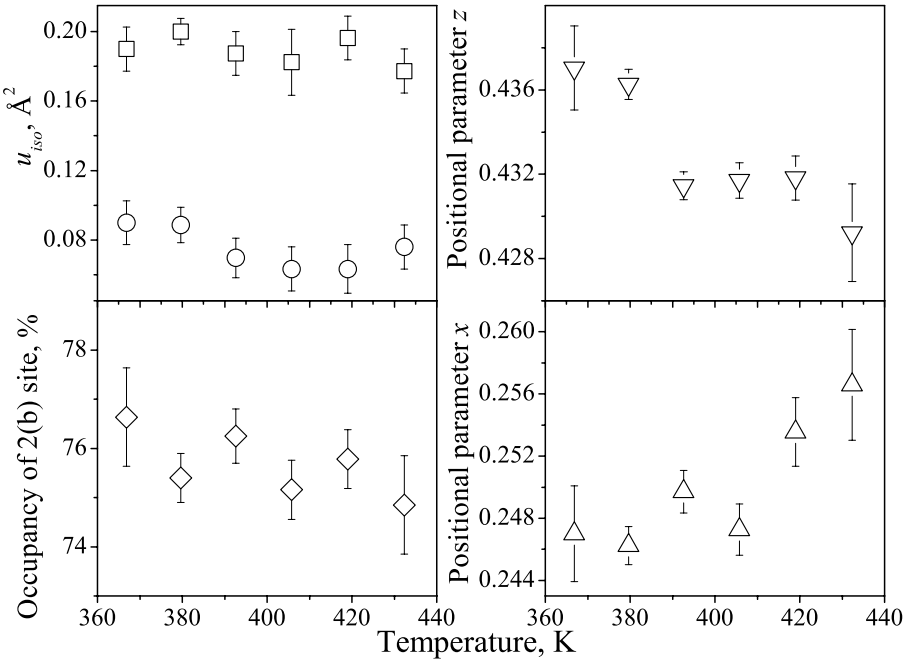

Figure 5.17: Temperature dependences of isotropic thermal parameters of S^{2-} (circles) and Ag^{+}/Cu^{+} (squares), normalized site occupation number of Cu^{+} on the triangular coordinated 2(b) site and cation positional parameters of 12(k) at (x, $2x$, z) sites of hexagonal α-AgCuS.

coordinations in the non-conducting phases was previously reported for AgI, Ag_2S and Cu_2S [91]. Besides, the change of the silver coordination from twofold in β-AgCuS and γ-AgCuS [50] to threefold in α-AgCuS should be noted. The cation-anion bond distances for hexagonal AgCuS at 380 K are 2.512(5) Å and 2.303(5) Å for Cu/Ag - S distances (*i.e.*, cations on 12(k) sites) and 2.397(5) Å for Cu - S distances (cations on 2(b) sites). This is in good agreement with the cation-anion bond distances for the orthorhombic phase, which range between 2.53-2.60 Å and 2.25-2.28 Å for Ag-S distances and from 2.24-2.27 Å and 2.31-2.35 Å for Cu-S distances.

5.3.3 Structural behaviour of superionic δ-AgCuS

The cation distribution in δ-AgCuS was parameterized using different structural models with silver and copper cations randomly distributed over tetrahedral and octahedral interstitial sites within a rigid sulphur fcc sublattice. Firstly, simultaneous Rietveld refinements based on synchrotron and neutron diffraction data collected for δ-AgCuS at 460 and 640 K, were performed. During refinement great care was taken to ensure that data were not overinterpreted by models with an inappropriate large number of structural parameters. Secondly, separate refinements were performed on the basis of synchrotron and neutron diffraction data at all temperatures individually. In summary the results of simultaneous and individual Rietveld refinements are consistent, although the moderate differences generated by the different scattering techniques and counting statistics can be observed.

Hence, simultaneous Rietveld refinements were based on a $Fm\overline{3}m$ symmetry and are summarized in tables 5.5, 5.6. The results reflect a considerable degree of cation disorder which can be modelled by a random occupation of the tetrahedral 8(c) site at $(\frac{1}{4}, \frac{1}{4}, \frac{1}{4})$ and the octahedral 32(f) site at (x, x, x) with $\frac{1}{3}<x<\frac{1}{2}$ (model 5, tables 5.5, 5.6). This model indicates cation disorder in $\langle 111 \rangle$ directions. It should also be noted that at $x\sim$0.37-0.38 cations are practically occupying 32(f) (x, x, x) sites on the boundary between tetrahedral and octahedral cavities but are noticeably shifted towards the centers of the octahedra. Therefore, the 32(f) site at (x, x, x) with $x\sim$0.37-0.38 is octahedral (figure 5.18). Attempts were also made to refine the data in the ideal antifluorite structure and in a "one-site" model with cations distributed in $\langle 111 \rangle$ directions in 32(f) at (x, x, x) with $\frac{1}{4}<x<\frac{1}{3}$ (see tables 5.5,

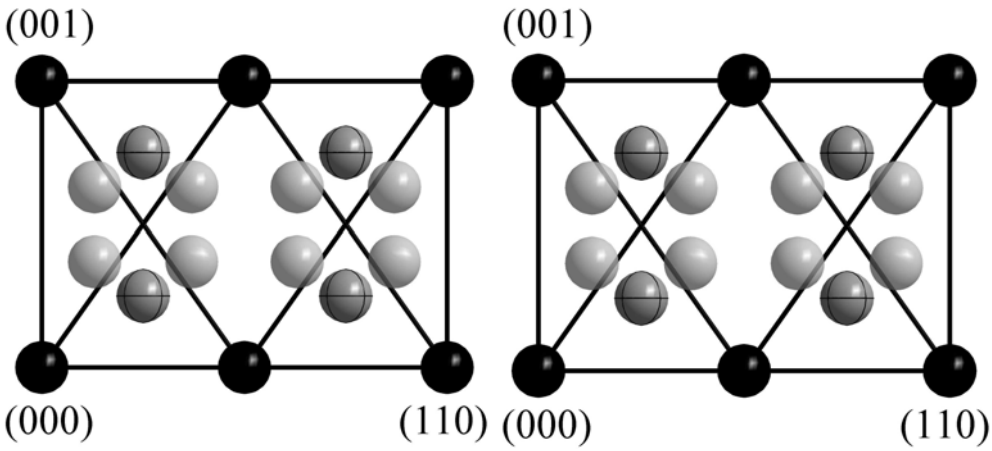

(a) δ-AgCuS at 460 K (b) δ-AgCuS at 640 K

Figure 5.18: Schematic representation of the average structure of fcc AgCuS. The plots show a (110) section through the unit cell and 100% occupancy for all crystallographic positions. The diagonal lines indicate the positions of the boundaries between tetrahedral and octahedral interstices. Black spheres, grey spheres with inner lines and grey spheres – S^{2-} in the 4(a), Ag^{+}/Cu^{+} in the 8(c) and Ag^{+}/Cu^{+} in the 32(f) sites, respectively.

5.6). The following models with cations distributed between two sites were tested: between 8(c) sites at ($\frac{1}{4}$, $\frac{1}{4}$, $\frac{1}{4}$) and 4(b) at ($\frac{1}{2}$, $\frac{1}{2}$, $\frac{1}{2}$) as well as between 32(f) at (x, x, x) with $\frac{1}{4}<x<\frac{1}{3}$ and 32(f) at (x, x, x) with $\frac{1}{3}<x<\frac{1}{2}$ (illustrating cation disorder in $\langle 111 \rangle$ direction); between 8(c) at ($\frac{1}{4}$, $\frac{1}{4}$, $\frac{1}{4}$) and 24(d) at (0, $\frac{1}{4}$, $\frac{1}{4}$) sites (disorder in $\langle 100 \rangle$ direction); between 8(c) at ($\frac{1}{4}$, $\frac{1}{4}$, $\frac{1}{4}$) and 48(i) at (x, x, $\frac{1}{2}$) with $\frac{1}{3}<x<\frac{1}{2}$ sites (disorder in $\langle 110 \rangle$ direction). All these models were either unstable in the refinement due to high correlations between the fitted parameters or produced a worse fit to the experimental data.

Table 5.5: A summary of the possible structure models used to interpret the diffraction data for the cubic δ-AgCuS phase at 460 K. Neutron and synchrotron diffraction data were treated simultaneously. χ^2 is the goodness of fit. The isotropic thermal parameters u_{iso} and positional parameters of the cations as well as the occupancy of cations on "split" positions were constrained during the refinements.

$Fm\bar{3}m$, Z=4, T=460 K, a=5.9564(6) Å							
Model	1	2	3	4	5	6	7
S, site	4(a) at (0,0,0)						
u_{iso} (Å^2)	0.023(1)	0.059(4)	0.454(4)	0.030(3)	0.139(13)*	0.197(16)	0.127(20)
Occupancy (%)	100	100	100	100	100	100	100
Ag/Cu, site	8(c)	32(f)	8(c)	8(c)	8(c)	8(c)	32(f)
x	$\frac{1}{4}$	0.324(5)	$\frac{1}{4}$	$\frac{1}{4}$	$\frac{1}{4}$	$\frac{1}{4}$	0.305(6)
y	$\frac{1}{4}$	0.324(5)	$\frac{1}{4}$	$\frac{1}{4}$	$\frac{1}{4}$	$\frac{1}{4}$	0.305(6)
z	$\frac{1}{4}$	0.324(5)	$\frac{1}{4}$	$\frac{1}{4}$	$\frac{1}{4}$	$\frac{1}{4}$	0.305(6)
u_{iso} (Å^2)	0.091(1)	0.304(12)	0.121(7)	0.333(7)	0.139(13)*	0.369(15)	0.116(20)
Occupancy (%)	100	25	68(1)	63.0(9)	26.8(9)	25.4(3)	11(3)
Ag/Cu, site	–	–	4(b)	24(d)	32(f)	48(i)	32(f)
x	–	–	$\frac{1}{2}$	0	0.370(5)	0.347(2)	0.375(3)
y	–	–	$\frac{1}{2}$	$\frac{1}{4}$	0.370(5)	0.347(2)	0.375(3)
z	–	–	$\frac{1}{2}$	$\frac{1}{4}$	0.370(5)	$\frac{1}{2}$	0.375(3)
u_{iso} (Å^2)	–	–	0.121(7)	0.333(7)	0.139(13)*	0.369(15)	0.116(20)
Occupancy (%)	–	–	64(1)	12.3(9)	18.3(9)	12.4(3)	13(3)
χ^2	14.3	11.0	15.8	15.0	6.3	7.9	8.3

*- during refinements u_{iso} of anions and cations have shown similar values at all considered temperatures, therefore, one overall thermal parameter was used in model 5.

Table 5.6: A summary of the possible structure models used to interpret the diffraction data for the cubic δ-AgCuS phase at 640 K. Neutron and synchrotron diffraction data were treated simultaneously. χ^2 is the goodness of fit. The isotropic thermal parameters u_{iso} and positional parameters of the cations as well as the occupancy of cations on "split" positions were constrained during the refinements.

$Fm\bar{3}m$, Z=4, T=640 K, a=5.9863(10) Å							
Model	1	2	3	4	5	6	7
S, site	4(a) at (0,0,0)						
u_{iso} (Å^2)	0.129(13)	0.228(25)	0.543(18)	0.139(25)	0.130(13)*	0.241(13)	0.151(12)
Occupancy (%)	100	100	100	100	100	100	100
Ag/Cu, site	8(c)	32(f)	8(c)	8(c)	8(c)	8(c)	32(f)
x	$\frac{1}{4}$	0.338(5)	$\frac{1}{4}$	$\frac{1}{4}$	$\frac{1}{4}$	$\frac{1}{4}$	0.304(9)
y	$\frac{1}{4}$	0.338(5)	$\frac{1}{4}$	$\frac{1}{4}$	$\frac{1}{4}$	$\frac{1}{4}$	0.304(9)
z	$\frac{1}{4}$	0.338(5)	$\frac{1}{4}$	$\frac{1}{4}$	$\frac{1}{4}$	$\frac{1}{4}$	0.304(9)
u_{iso} (Å^2)	0.725(19)	0.485(25)	0.156(18)	0.583(25)	0.130(13)*	0.481(12)	0.089(12)
Occupancy (%)	100	25	63(1)	57.3(8)	31.3(10)	28.2(4)	8.6(7)
Ag/Cu, site	–	–	4(b)	24(d)	32(f)	48(i)	32(f)
x	–	–	$\frac{1}{2}$	0	0.369(5)	0.335(2)	0.384(7)
y	–	–	$\frac{1}{2}$	$\frac{1}{4}$	0.369(5)	0.335(2)	0.384(7)
z	–	–	$\frac{1}{2}$	$\frac{1}{4}$	0.369(5)	$\frac{1}{2}$	0.384(7)
u_{iso} (Å^2)	–	–	0.156(18)	0.583(25)	0.130(13)*	0.481(12)	0.089(12)
Occupancy (%)	–	–	74(1)	14.2(8)	17.2(10)	12.0(4)	16.5(7)
χ^2	12.4	11.2	17.6	10.5	8.1	10.1	10.1

*- during refinements u_{iso} of anions and cations have shown similar values at all considered temperatures, therefore, one overall thermal parameter was used in model 5.

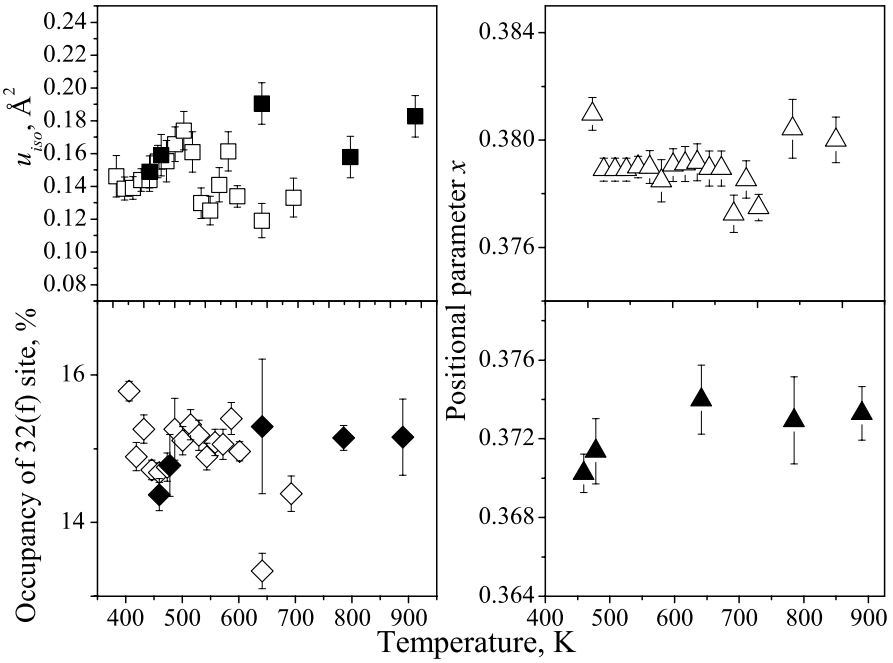

Figure 5.19: Temperature dependences of overall thermal parameters, normalized site occupation number of Ag^+/Cu^+ residing on the 32(f) site and cation positional parameter of 32(f) sites within the cubic δ-AgCuS in model 5 from tables 5.5 and 5.6. Open symbols – synchrotron data (B2), close symbols – neutron data (SPODI).

The model with a random occupation of the tetrahedral 8(c) site at ($\frac{1}{4}$, $\frac{1}{4}$, $\frac{1}{4}$) and the octahedral 32(f) site at (x, x, x) with $\frac{1}{3}<x<\frac{1}{2}$ yields no significant temperature dependence for all relevant parameters of the average structure: neither the overall temperature factor, u_{ov}, nor the cation positions on the octahedral site 32(f) at (x, x, x) with $\frac{1}{3}<x<\frac{1}{2}$, nor the cation occupancies change significantly with temperature (see figure 5.19). Within this model, disorder occurs in $\langle 111 \rangle$ directions towards the faces of octahedra rather than to its edges; in spite of the significant octahedral occupation, there is only a minimal cation density on the ideal octahedral site 4(b) at ($\frac{1}{2}$, $\frac{1}{2}$, $\frac{1}{2}$). In the light of these structural features, it is likely that cations jump in skewed $\langle 100 \rangle$ directions between nearest-neighbour tetrahedral sites *via* the peripheries of the octahedral cavities. The same mechanism of ionic conductivity was proposed on the basis of powder diffraction studies for the superionic antifluorite phases of Ag_2Te [86], $Cu_{2-\delta}Se$ (δ=0, 0.15, 0.25) [57] and AgCuSe [48]. Note that diffraction results on a number of copper- and silver- based chalcogenides and halides (for instance, [48, 57, 88, 89]) imply that ionic conductivity can be sensitive to details of the cation redistribution between available interstitial sites *vs.* temperature as well as to the stoichiometry of the

material. Taking this into account, we can propose a correlation between the results of the electrochemical measurements from Kadrgulov *et al.* [15] on one hand, which revealed only a relatively modest increase in the ionic conductivity with temperature within the stability range of δ-AgCuS, and the diffraction results on the other hand, which show no pronounced cation redistribution in this temperature range. The same correlation was also reported for superionic fcc-AgCuSe [48] and for superionic fcc-$Ag_xPb_{1-x}I_{2-x}$ with x=$\frac{1}{3}$ and $\frac{2}{3}$ [88]. Dramatic changes in the ionic conductivity with temperature seem to require a redistribution of cations.

5.4 High-temperature synchrotron powder diffraction on jalpaite, Ag_3CuS_2

5.4.1 Phase transitions of Ag_3CuS_2

The analysis of the structural behaviour of Ag_3CuS_2 showed the following phase transitions at elevated temperatures: tetragonal $I4_1/amd \overset{387K}{\longrightarrow}$ cubic $Im\bar{3}m \overset{483K}{\longrightarrow}$ cubic $Im\bar{3}m$ plus cubic $Fm\bar{3}m \overset{549K}{\longrightarrow}$ cubic $Fm\bar{3}m$. A large decrease in peak intensity after the tetragonal $I4_1/amd \overset{387K}{\longrightarrow}$ cubic $Im\bar{3}m$ phase transformation indicates a high degree of structural disorder introduced by transition. Following the notation accepted for other superionic conductors (see for instance [90] and [58]), the RT structure of Ag_3CuS_2 should be denoted as β-Ag_3CuS_2, the cubic bcc phase as α-Ag_3CuS_2 and the cubic fcc phase at the temperature immediately above the α-phase should be denoted as δ-Ag_3CuS_2.

The transition temperature of $\beta \overset{387K}{\longrightarrow} \alpha$ and the lowest temperature of the single phase stability range of δ-Ag_3CuS_2 (549 K) are in good agreement with the results presented in [54, 55]. The beginning of the two phase region α plus δ at 483 K was, however, not determined in [55], whereas the coexistence region of two cubic α and δ phases was not revealed in [54]. The analysis of the diffraction pattern from the sample after heat treatment in argon during the diffraction measurements, showed no changes with respect to the initial state. The sample melts between 973 and 1023 K.

Examples of diffraction patterns of Ag_3CuS_2 at different temperatures are shown in figure

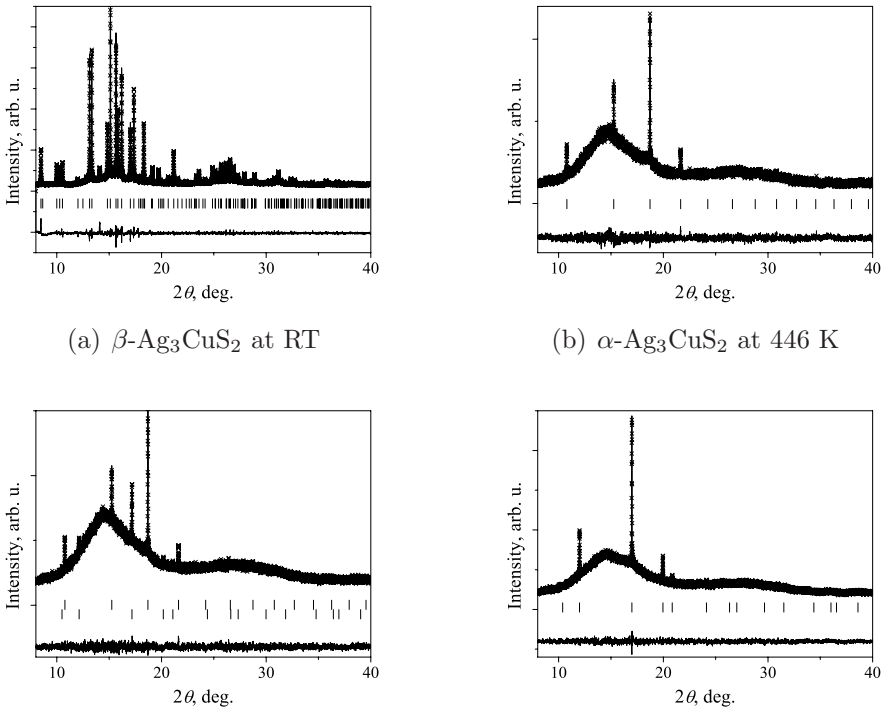

(a) β-Ag_3CuS_2 at RT

(b) α-Ag_3CuS_2 at 446 K

(c) α + δ-Ag_3CuS_2 at 487 K

(d) δ-Ag_3CuS_2 at 745 K

Figure 5.20: Results of indexing on Ag_3CuS_2 for data collected with B2 diffractometer (profile matching mode). Crosses are experimental data, the lines through the crosses are calculated profiles and tick marks show the calculated positions of Ag_3CuS_2 reflections.

5.20. The drawn lines are the results of profile matching calculations, which confirm the correct indexing, *i. e.* the correct unit cell metric, but do not take any atom positions into account.

5.4.2 Anomalous thermal expansion in Ag_3CuS_2 and some of the other superionics

The lattice parameters, cell axial ratio c/a and cell volume per mole formula unit of jalpaite as a function of temperature are illustrated in figure 5.21. Negative thermal expansion in c-direction was observed in β-Ag_3CuS_2, whereas no anomalies in the thermal expansion in a-direction were revealed. Additionally, the axial c/a ratio showed a reduction with increasing temperature, *i.e.* distortions in bcc lattice decrease with temperature increase. The discontinuous volume changes (see figure 5.21) of about 0.77% at the $\beta \longrightarrow \alpha$ and 0.58% at $\alpha \longrightarrow \delta$ transformations are a very strong indication for a 1st order phase transition. The volume thermal expansion is linear in tetragonal and fcc phases of jalpaite with coefficients

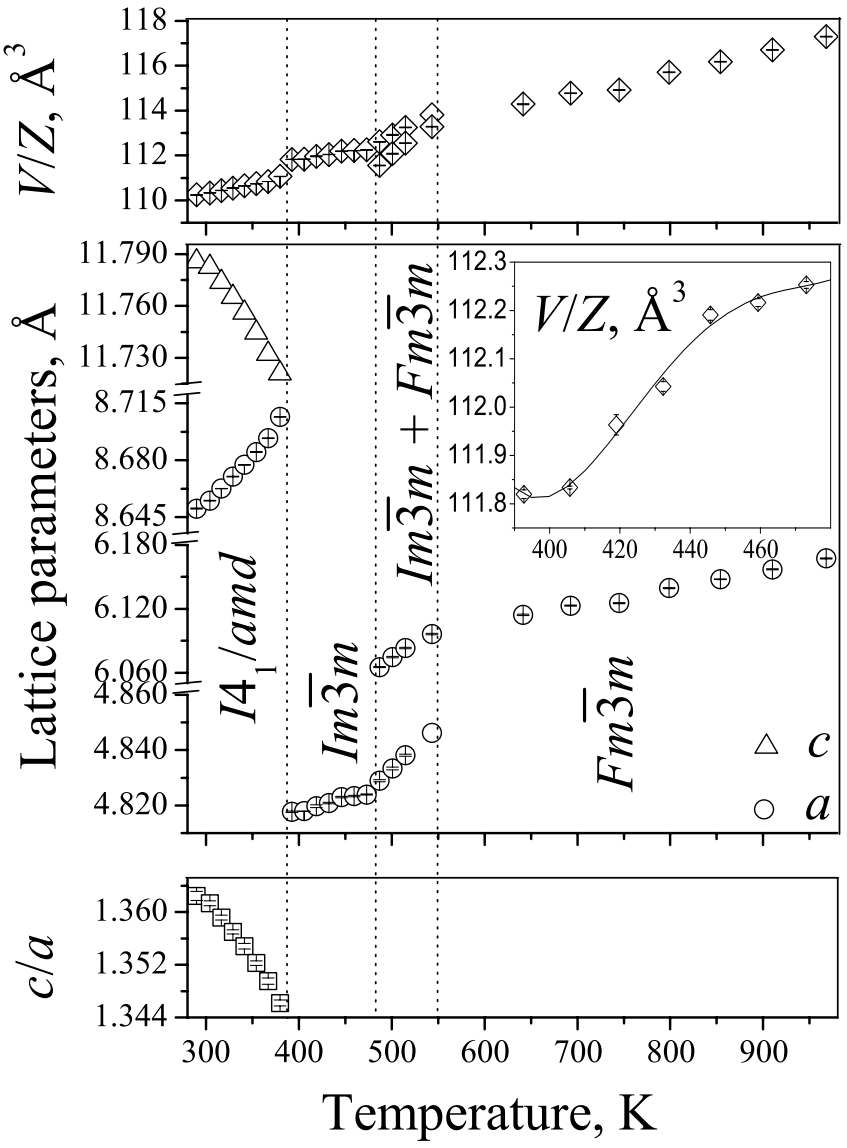

Figure 5.21: The unit cell axial ratio c/a, cell dimensions a, c and unit cell volume per formula unit V/Z of jalpaite Ag_3CuS_2 as a function of temperature in the range from RT up to melting point. Inset: unusual thermal expansion in bcc α-Ag_3CuS_2.

of $78{\cdot}10^{-6}K^{-1}$, and $80{\cdot}10^{-6}K^{-1}$, respectively. A non-linear thermal expansion was revealed in bcc-Ag_3CuS_2 (see inset in figure 5.21).

It should be noted that an anomalous thermal expansion seems to be characteristic for other superionics. The negative thermal expansion in c-direction was detected in some other superionic conductors by powder diffraction, for instances, in hexagonal β-AgI [92], β-CuI [93], α-AgCuS [58, 63], orthorhombic β-AgCuS [58, 63] as well as in rhombohedral Ag_3AsS_3 and Ag_3SbS_3 [94],*etc.* The changes in the c/a ratio towards the 'ideal' values were also reported for superionic compounds as hexagonal β-CuI [87, 93] and α-AgCuS [58],

pseudo-hexagonal orthorhombic β-Ag_2ZnI_4 [88] and β-AgCuS [58,63], tetragonal β-Cu_2HgI_4 and β-Ag_2HgI_4 [95] and also indicated from the results in [92] for hexagonal β-AgI.

An explanation of the negative thermal expansion along the c-axis of β-AgI was successfully given in terms of a coupling between a cluster pair of mobile ions and local static distortions [96, 97]. In the frame of this approach, the positive or negative expansion of Ag–I distances with temperature depends on the magnitude of static and dynamic distortions. The dynamical distortion in β-AgI is larger than the static distortion in most of the temperature range, and so a positive expansion occurs as usual. Nevertheless, a negative thermal expansion was observed in a limited temperature range around the temperature of the superionic phase transition [92]. This effect results from a static local distortion, larger than the dynamic distortion since a number of vacancies are excited close to the transition temperature. In analogy, the change of a positive expansion along the c-axis into a negative value in β-AgCuS as well as the negative thermal expansion along the c-direction in α-AgCuS and β-Ag_3CuS_2 can be explained in terms of cluster-induced local distortions as well. Such a model of defect-induced unusual thermal expansion in AgCuS and Ag_3CuS_2 can be modelled by molecular dynamics simulations. An example of such modelling applied to β-AgI is well described in reference [98]. It was shown that the anomalous decrease of the c-axis of β-AgI with temperature increase correlates with the excitation of defects. The application of this model to check the universality of the ion-cluster coupling with distortions is, however, beyond the scope of this work.

Chapter 6

Results of inelastic neutron scattering

Lattice dynamics and diffusion in superionic conductors are closely related. In particular, it is assumed that diffusion in superionics can be considered as a process connected with the lowest-energy optic mode observed in the vibrational spectra of superionics (see for instance [99–104]). Low-energetic excitations have been observed by inelastic neutron scattering in the low-temperature phase of cation conducting superionics and it was suggested that the low-energy mode is connected with the localized vibration of the conducting type of ion [36] or with low-energy flat transverse acoustic phonons [105, 106]. Wakamura considered lattice dynamics in superionics based on a linear chain with two kinds of atoms [105, 106]. He showed that the value of low-energy excitation is related to the frequency of the transverse zone-edge acoustic phonon. This leads to the proportionality of $E_{LE} \sim \frac{1}{\sqrt{m}}$, where m is the heavier atomic mass. Recently, Sakuma confirmed on the basis of INS results that the values of the low-energy excitation depend on the mass of the heaviest ion in the compound as $\sim \frac{1}{\sqrt{m}}$ and does not depend on the mass of the conducting ions [101].

It is important to consider also another approach to the low-energy mode in superionic conductors proposed by Boyer [107,108]. He has provided an explanation for superionicity in CaF_2 in terms of the high-temperature instability of a perfect lattice. It is argued, that the softening of the lowest-energy mode in CaF_2 is related to the onset of the ionic conductivity, since both effects occur at similar temperatures and lattice constants. CaF_2 has fluorite structure similar to many other superionic conductors where a low-energy mode has been observed [36,99,100,105,106]. At the low-energy mode fluorine anions move along the cubic-

axes directions with cage cations at rest. It is apparently of importance that neighboring chains move out of phase. In this case fluorine ions can move in the cubic axes directions without restriction. In order to overcome the challenge of a too small amplitude of the low-energy mode in comparison with minimal distance between two tetrahedral sites, Boyer has suggested that mobile ions are mainly disordered mostly over tetrahedral sites, should first move in the direction to the empty octahedral sites to reduce the large potential barrier and after that jump on a vacant adjacent tetrahedral site. This proposed mechanism of diffusion agrees with numerous results [2, 48, 57, 86, 87] *etc.* (see previous chapter as well), where a diffusion pathway of mobile ions in fcc superionic conductors along the tetrahedral sites in skewed $\langle 100 \rangle$ directions through the peripheries of octahedral cavities was suggested.

Lattice dynamics and in particular the low-energy modes are doubtless a key to understand the phenomenon of superionicity. However, the role of the low-energy modes in superionic conductor is still not clear. For example, recent INS measurements performed on both a single-crystal and on polycrystalline superionic $Cu_{2-\delta}Se$ have shown no low-energy optic mode, though transverse acoustic modes in β-$Cu_{1.85}Se$ are unusually flat over the major part of the Brillouin zone [36]. In this chapter the results of inelastic neutron scattering studies of the lattice dynamics in polycrystalline β- and α- AgCuSe and β- and α- AgCuS superionic conductors [48, 59] are reported.

6.1 Inelastic neutron scattering on AgCuSe

6.1.1 Short discussion of $S(Q, \varepsilon)$ spectra

The $S(Q, \varepsilon)$ spectra after the standard data reduction procedure at DIN-2PI are presented in figure 6.1 for some selected values within the accessible kinematical range. $S(Q, \varepsilon)$ spectra of non-superionic β-AgCuSe consist of a narrow elastic component, centered around zero energy transfer, and a broad inelastic one. Note the absence of any pronounced traces of low-energy excitations in the $S(Q, \varepsilon)$ spectra of β-AgCuSe. In reference [109] the existence of such low-energy excitations in Cu- and Ag-based superionics are reported, but appear only just below the superionic phase transition. In reference [106] was shown that such a low-energy mode is assigned to an optical phonon at the lowest frequency, originating from a

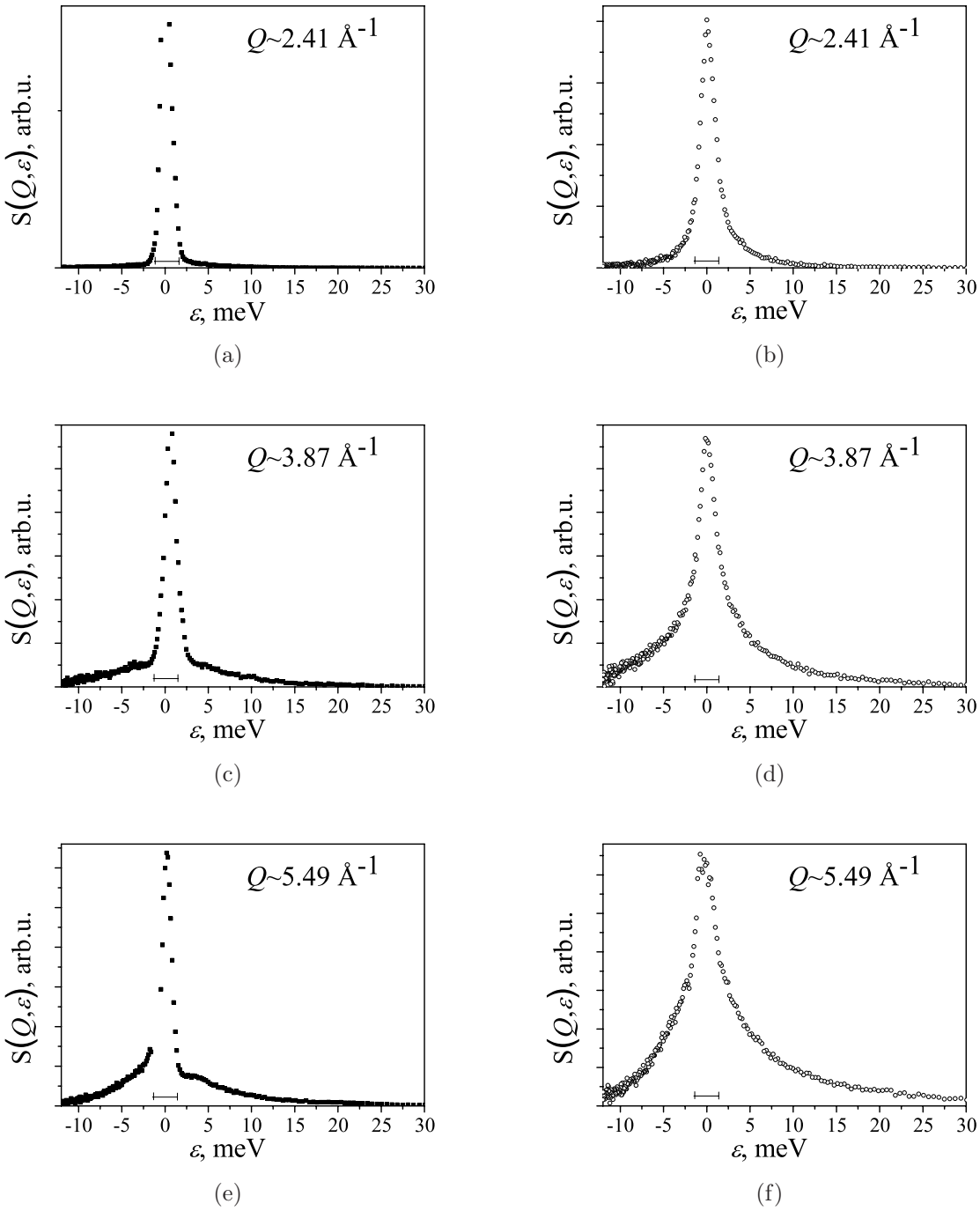

Figure 6.1: The $S(Q, \varepsilon)$ spectra after standard data reduction at DIN-2PI for β-AgCuSe at T=285 K (left column) and α-AgCuSe at T=505 K (right column), collected with an initial energy of 18.496 meV. Spectra for selected Q-values in the beginning, middle and the end of the kinematical range are shown. The asymmetry of the spectra is caused by a gradual variation of momentum transfer with energy transfer as well as by coherence effects. Energy resolution is marked in the figure by the pointer around $\varepsilon \sim 0$.

transverse-zone-edge acoustic phonon. Specific properties of this mode, such as pressure and temperature dependences of the mode frequency as well as a proportionality of the mode frequency with inverse square root of the mobile ion mass are discussed in the latter work. From an analysis of the data from [106] for numerous ternary Ag-based superionics with two kind of mobile ions, where silver is the heavier mobile ion (for instance, KAg_4I_5, $RbAg_4I_5$ and $NH_4Ag_4I_5$), a proportionality of the mode energy (about 2 meV) and the square root of the silver ion mass is evident. Therefore, we can suppose the existence of a low-energy optic mode at an energy transfer about 2 meV in non-superionic β-AgCuSe. The overlap at this energy transfer with the strong elastic peak can be the main reason, why no traces of low-energy excitations were observed in the $S(Q, \varepsilon)$ spectrum, measured by inelastic neutron scattering. Experiments with better resolution are necessary to decide unambiguously about the existence or absence of such low-energy excitations.

The spectra of α-AgCuSe are qualitatively similar with spectra of superionic silver iodide [104, 110], silver selenide or silver telluride [111]: in these spectra, in addition to the elastic (Bragg) and inelastic components, low energy scattering is observed, which is centered at zero energy transfer. In the present case such quasi-elastic scattering results from the diffusive motion of copper and silver ions. In reference [110] quasi-elastic scattering of silver ions in superionic silver iodide was analyzed based on superposition of a random local motion and translational jump diffusion. The interpretation of quasi-elastic neutron scattering spectra from AgCuSe is limited by the large absorption cross section of silver, requiring long beam time for a high-resolution experiment, and an important coherent contribution to the totally scattered intensity. Furthermore, the knowledge of the incoherent elastic structure factor from additional diffuse scattering experiments is necessary.

6.1.2 Generalized neutron-weighted densities of states in β- and α-AgCuSe

In order to investigate the changes in the frequency spectrum of AgCuSe accompanied with the superionic phase transitions, the substraction of multiphonon contributions is necessary first. This was done as described in the experimental part of this thesis (chapter 3). Multiphonon effects are illustrated in figure 6.2, where the densities of states at three different Q-

values are shown, resulting from an iterative process, converged after three iterations. Three phonons were used to build a multiphonon expansion series. The increase of multiphonon contributions at higher values of momentum transfer and with increasing temperature due to the increasing Debye-Waller factor is emphasized.

Neutron-weighted densities of states, $G(\varepsilon)$, for both phases are presented in figure 6.3. The spectra of $G(\varepsilon)$ in β- and α-AgCuSe can be described as a superposition of two well-defined broad peaks at energy transfers ε of about 8 and 18 meV. The linear (instead of a square) dependence of $G(\varepsilon)$ in the energy transfer range of $2.5 < \varepsilon < 5$ meV for both phases is particularly noteworthy. Such non-Debye behaviour of $G(\varepsilon)$ at low energies is an evidence of the high level of anharmonicity in a system.

The temperature effects usually manifest themselves in a phononic broadening [112]. Such a phonon broadening in superionics is commonly attributed to increasing anharmonic effects and time-averaged static disorder (see for example, [112, 113]). Moreover, increasing phonon-phonon scattering due to increasing phonon occupancies at higher temperatures play a crucial role in phonon broadening (see for example, [114]). This phonon broadening is reflected in the phonon density of states as a general smearing out of well defined features and a high-energy cut-off. Therefore, apparent changes in the frequency spectrum of superionic α-AgCuSe such as damping of the low-energy part (peak at $\sim$8 meV) and smearing of the high-energy part (peak at $\sim$18 meV) of the spectrum are clearly visible in contrast to the spectrum of non-superionic β-AgCuSe. Such changes in the frequency spectrum of the α-phase cannot only arise from temperature effects on phonons mentioned above. In the present case they are accompanied by a 1st order superionic phase transition. Moreover, the noticeable excess in the density of states in superionic α-AgCuSe above 23–25 meV is clearly visible. Such an effect has to be handled with care, because the corresponding energy range lies above the thermal energy, kT, for β-AgCuSe. These phonon states are not thermally populated, but the measurements were performed in upscattering (phonon annihilation) mode. This density of states can result from a thermal population of these phonon states in α-AgCuSe. Nevertheless, it should be noted that the dependence of the inelastic intensity in the upscattering regime is usually influenced by instrumental or thermal effects in those kinds of neutron experiments. In the present case, these effects were taken

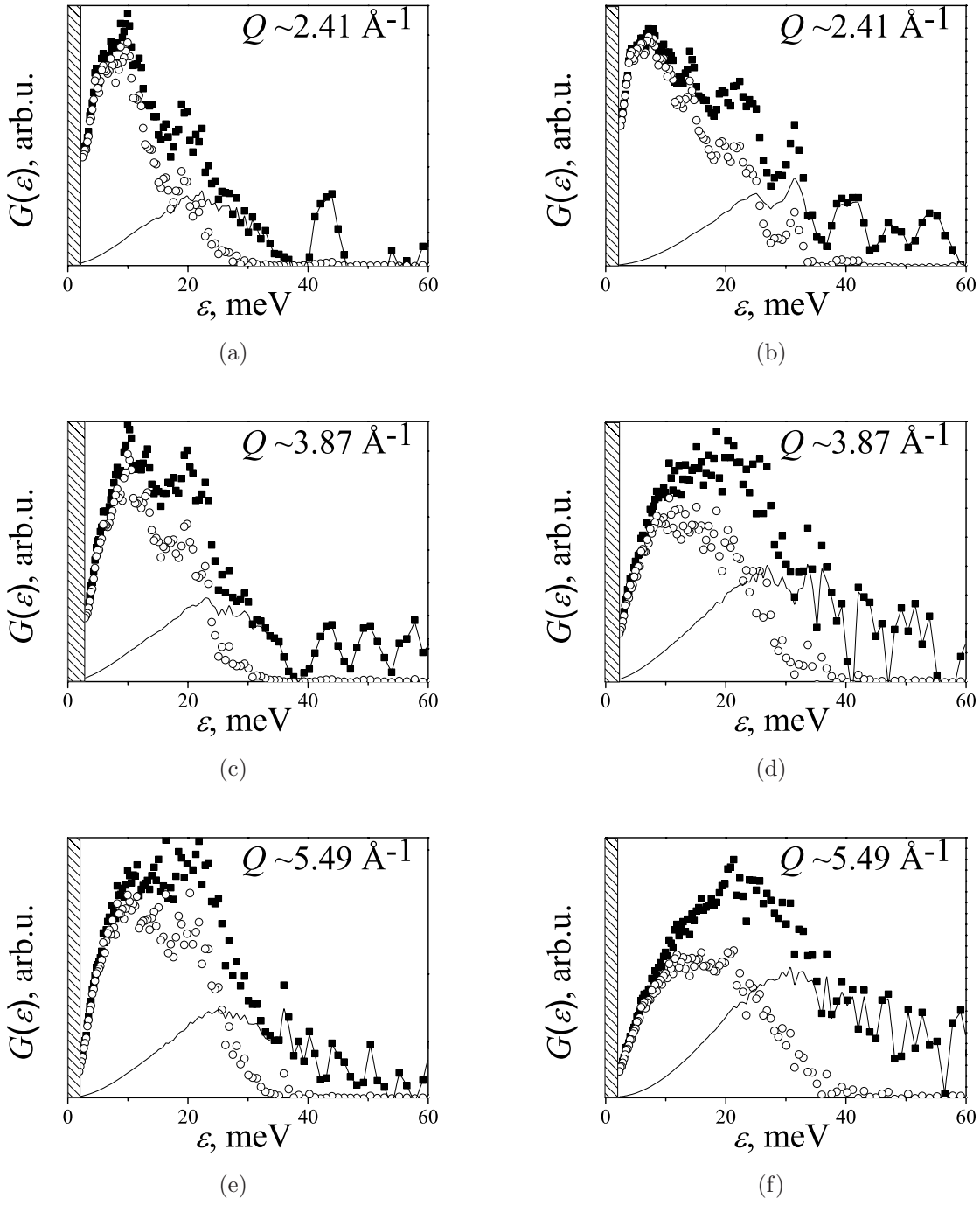

Figure 6.2: Multiphonon effects for β-AgCuSe at 285 K (left column) and α-AgCuSe at 505 K (right column) for selected Q-values; empty symbols - one-phonon scattering, thin lines - multiphonon scattering, filled symbols - total contribution. The dashed area corresponds to the energy range with a pronounced overlap with the elastic peak.

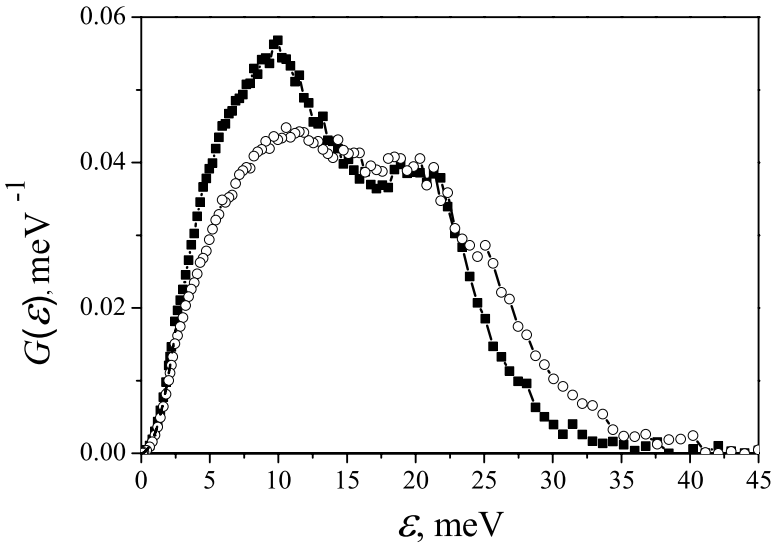

Figure 6.3: Neutron-weighted density of states of non-superionic β-AgCuSe at 285 K (filled squares) and superionic α-AgCuSe at 505 K (empty circles).

into account during data analysis by implementation of the thermal population factor and a multiphonon correction procedure. Nevertheless, in [79] it is shown that a smearing of the high-energy part of the spectra — above 23–25 meV in our case — can probably be nothing else but a mathematical problem of data reduction during subtracting of the multiphonon effects. Hence, the excess of the density of states above 23–25 meV in α-AgCuSe is rather a mathematical problem in data reduction during the subtraction of the multiphonon terms than a physical effect. However, the description of the self-consistent iterative procedure as well as the weakness of such a correction is not the topic of this thesis and discussed elsewhere [75, 79, 80].

6.2 Inelastic neutron scattering on AgCuS

6.2.1 Inelastic neutron scattering spectra of $S(\Theta, \varepsilon)$ and $G(\Theta, \varepsilon)$ in AgCuS

The inelastic neutron scattering spectra in terms of both, the dynamic structure factor $S(\Theta, \varepsilon)$ and the generalized energy distribution function $G(\Theta, \varepsilon)$ were analysed. A comparative analysis of the $S(\Theta, \varepsilon)$ and $G(\Theta, \varepsilon)$ is useful, because of different weighting schemes in the

derivation from the double-differential cross section $\frac{d^2\sigma}{d\Omega d\varepsilon}$. $S(\Theta, \varepsilon)$ is proportional to $\frac{d^2\sigma}{d\Omega d\varepsilon}$ with a factor $\sim \frac{1}{\sqrt{E}}$ and $G(\Theta, \varepsilon)$ with a factor $\sim \sqrt{E}$. The low-energy modes are better analyzed using $S(\Theta, \varepsilon)$, whereas excitations at higher energies are better observed in $G(\Theta, \varepsilon)$. Inelastic neutron scattering spectra, expressed as the dynamic structure factor $S(\Theta, \varepsilon)$ and the generalized energy distribution function $G(\Theta, \varepsilon)$, are shown for α- and β-AgCuS in figures 6.4, 6.5, 6.6 and 6.7. Multiphonon effects (see figures 6.5, 6.6 and 6.7) were always calculated and subtracted as described in chapter 3.

Figure 6.4 shows the low energy peaks at $\varepsilon \sim 2.6$ and 6 meV in $S(\Theta, \varepsilon)$ of β-AgCuS. Peaks at 2.6 meV are seen at both sides of the spectra – the neutron energy gain and the neutron energy loss. The existence of this low-energy peaks agrees well with the results of references [101, 105, 106, 109]. Accordingly, the low-energy excitation scales with the mass of the heaviest ion of the superionic compound as $\sim \frac{1}{\sqrt{m}}$ (Ag^+ is the heaviest ion of the AgCuS, *i.e.*, according to the above mentioned references, low-energy excitation in this compound should appear at $\varepsilon \sim 2$ meV). Peaks near 6 meV are only for neutron energy gain because of the vicinity to the upper end of occupied states in the spectra. It is significant that modes corresponding to the peaks at $\varepsilon \sim 2.6$ and 6 meV show dispersionless behavior (see also figure 6.8). At energies higher than 6 meV, the intensity in $S(\Theta, \varepsilon)$ is too low to be analyzed in detail. However, peaks at $\varepsilon \sim 10$ meV can be detected in some spectra. At 348 K the intensity in $S(\Theta, \varepsilon)$ increases, especially at the neutron energy gain part of the spectra. At the same time no drastic changes in the line-shape of the spectra or shifts in the peak positions take place as the temperature of the sample is increased from 298 to 348 K. In contrast the temperature increase to 398 K changes the $S(\Theta, \varepsilon)$ spectra of α-AgCuS drastically. The low-energy part of $S(\Theta, \varepsilon)$ merges with the elastic peak to become an unified broad energy distribution centered at 0 meV (quasielastic scattering as in the case of α-AgCuSe) with long tails up to 15-20 meV. The changes in $S(\Theta, \varepsilon)$ at the $\beta \longrightarrow \alpha$ phase transition are most probably caused by a softening of the low energy modes with a simultaneous increase of the peak width.

The $G(\Theta, \varepsilon)$ spectra in β-AgCuS are similar for all scattering angles and coincide for 298 and 348 K within counting statistics. In the case of purely incoherent scattering $G(\Theta, \varepsilon)$ should be independent on the scattering angle. The difference between $G(\Theta, \varepsilon)$ in AgCuS

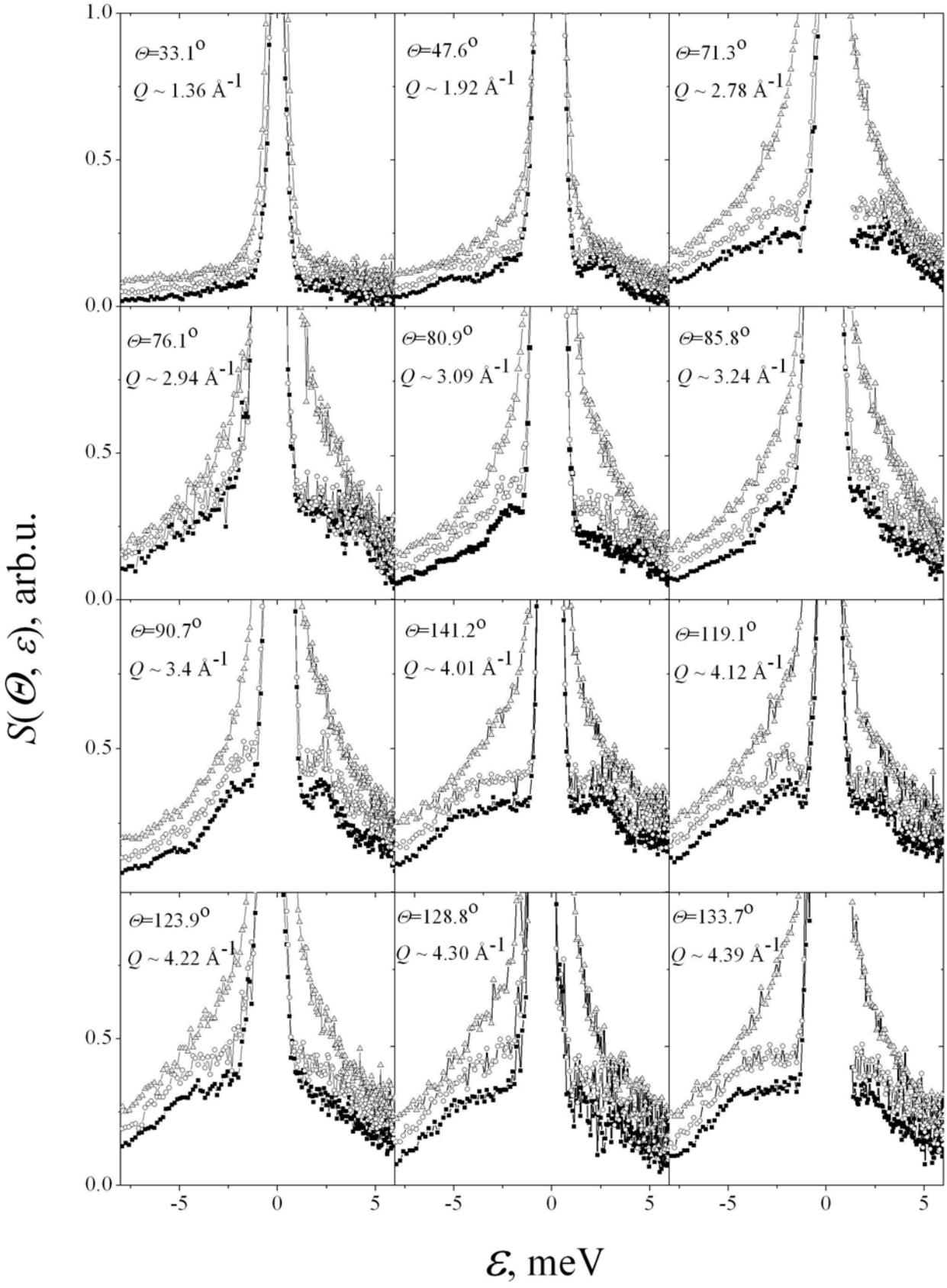

Figure 6.4: Dynamic structure factor $S(\Theta, \varepsilon)$ in AgCuS at 298 (filled squares), 348 (empty circles) and 398 K (triangles); spectra are shifted up against each other by 0.025 for clarity. The specific values for Q corresponds to the momentum transfer at $\varepsilon = 0$ meV.

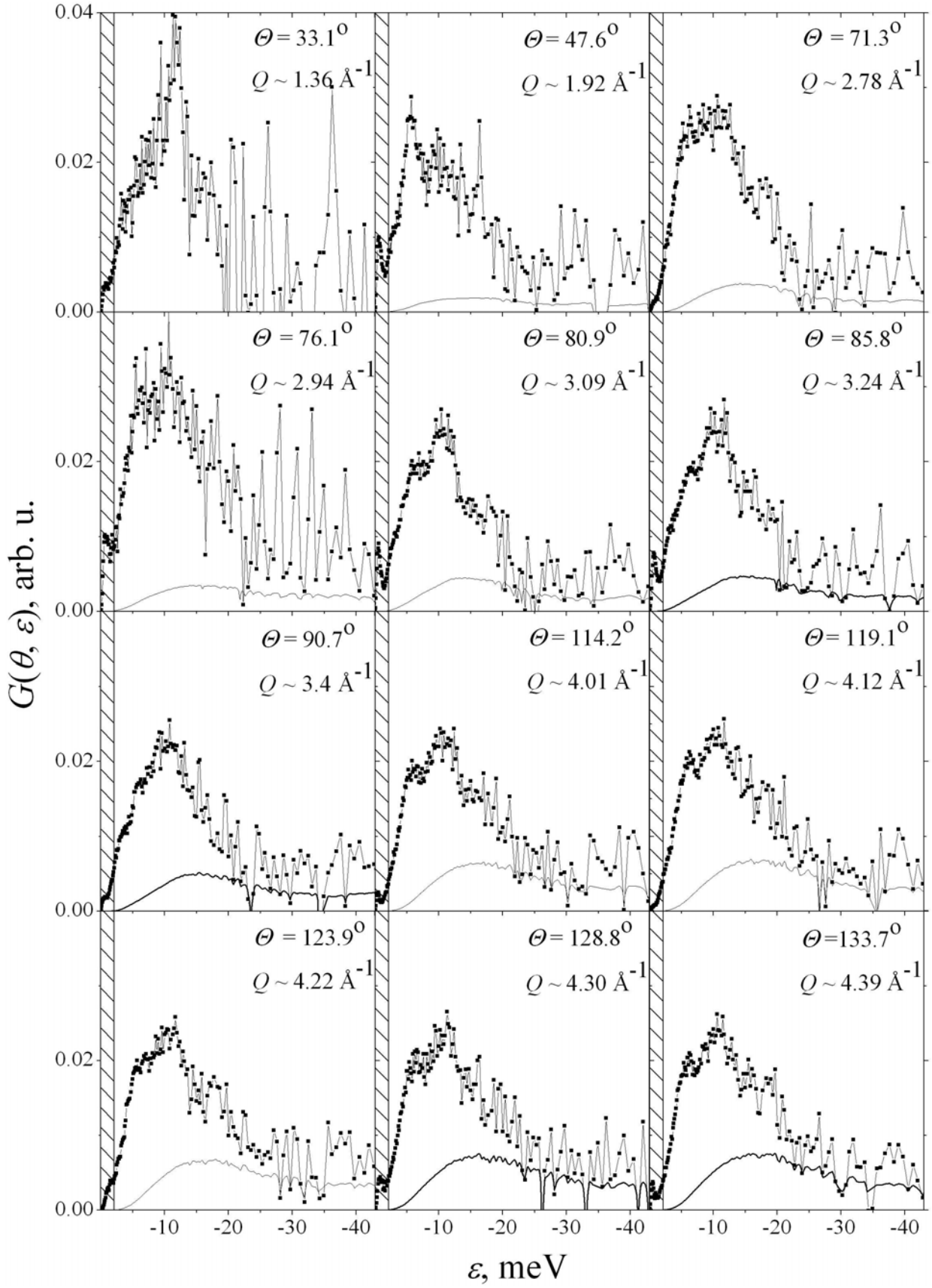

Figure 6.5: $G(\Theta, \varepsilon)$ spectra of orthorhombic β-AgCuS at RT (filled squares). Solid lines correspond to multiphonon contributions. Dashed areas correspond to the energy range of the elastic peak.

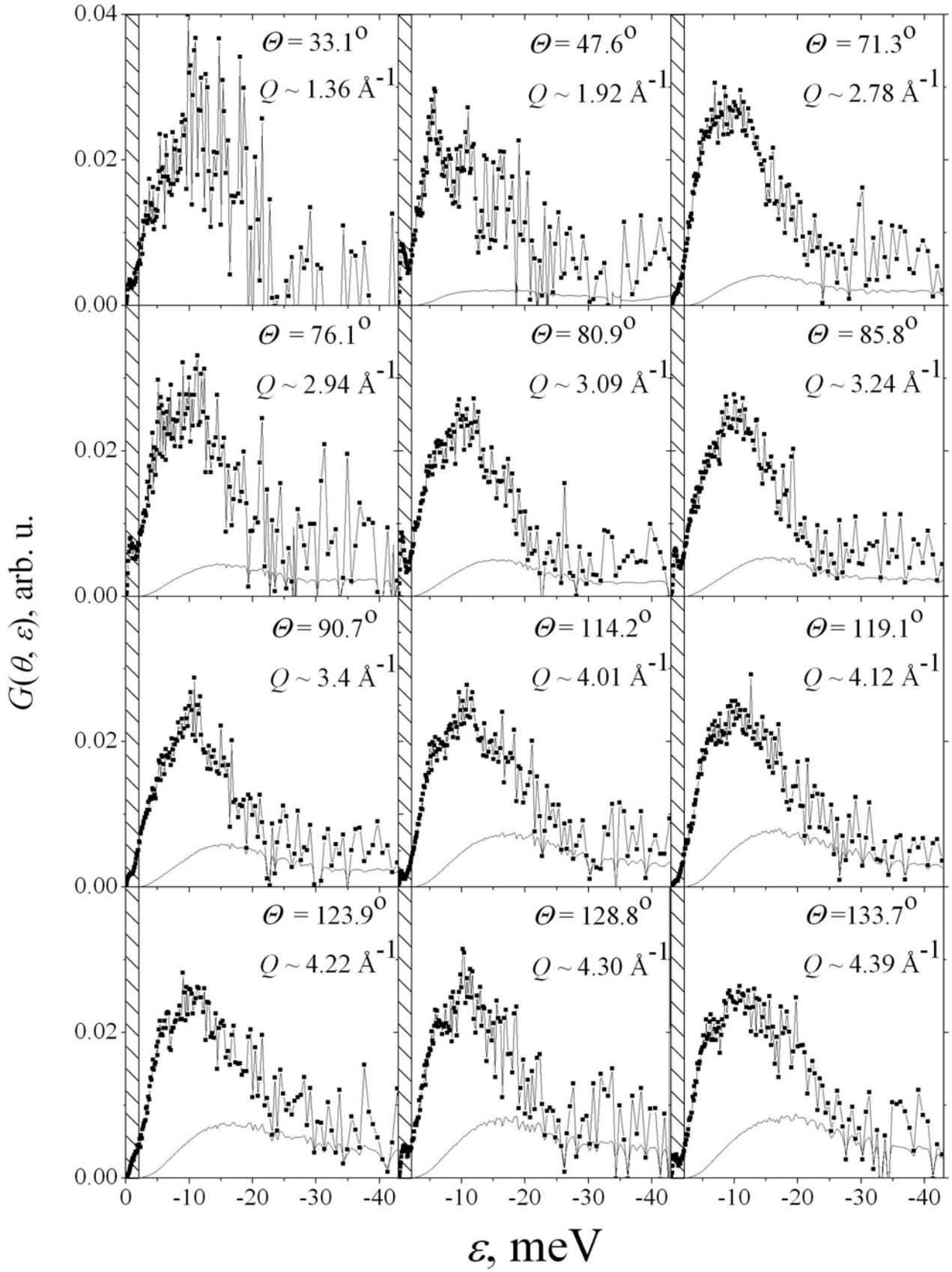

Figure 6.6: $G(\Theta, \varepsilon)$ spectra of orthorhombic β-AgCuS at 348 K (filled squares). Solid lines correspond to multiphonon contributions. Dashed areas correspond to the energy range of the elastic peak.

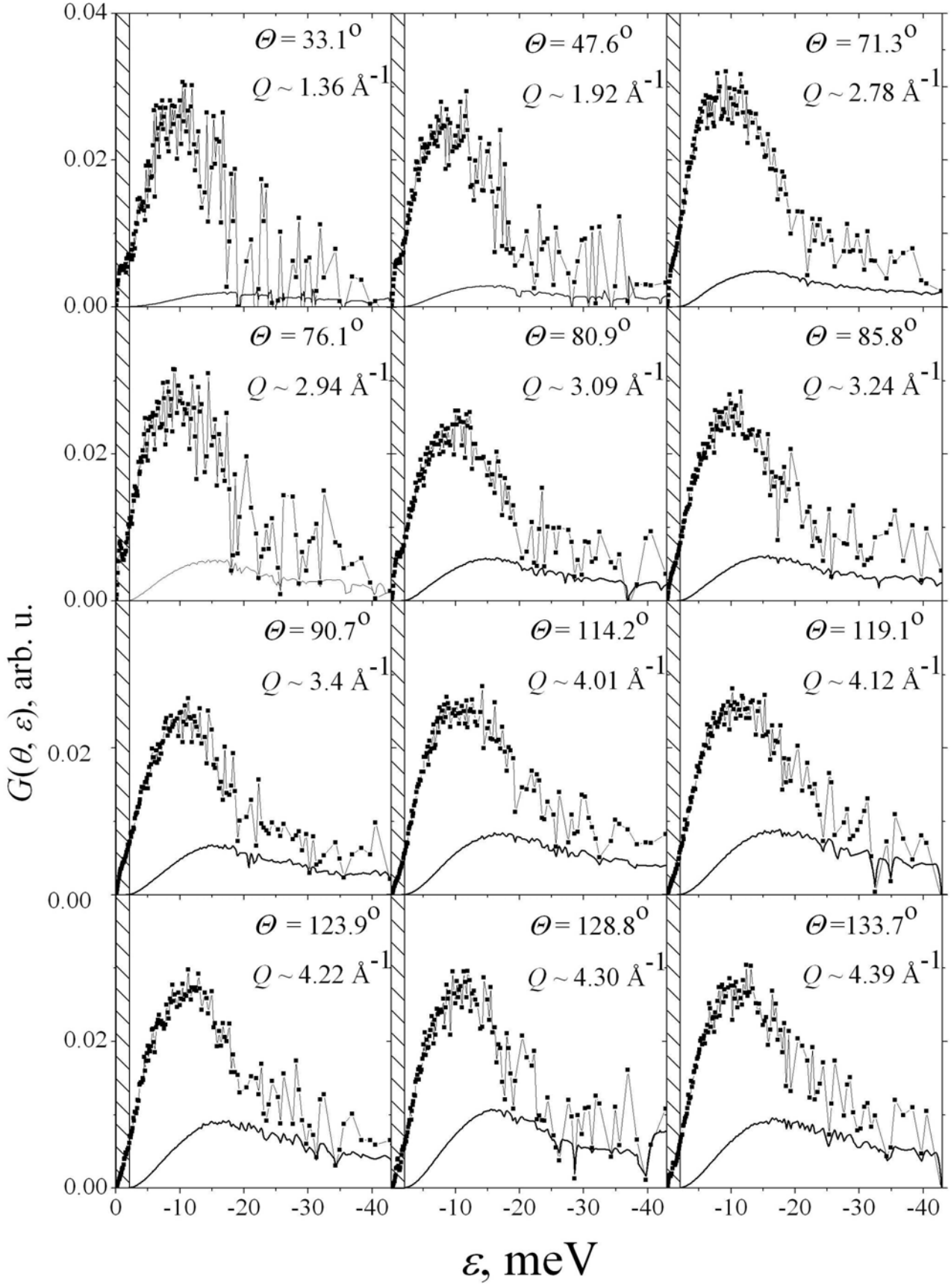

Figure 6.7: $G(\Theta, \varepsilon)$ spectra of hexagonal α-AgCuS at 398 K (filled squares). Solid lines correspond to multiphonon contributions. Dashed areas correspond to the energy range of the elastic peak.

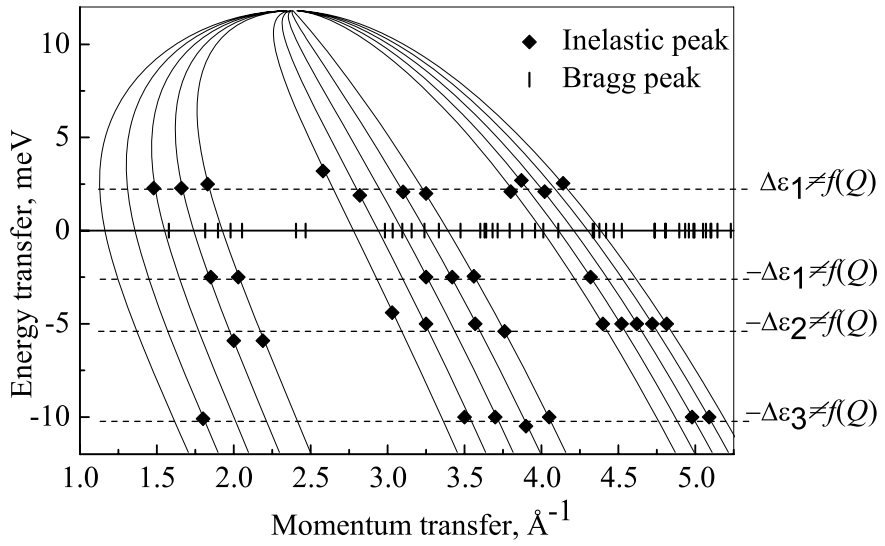

Figure 6.8: Position of the inelastic peaks observed in β- AgCuS together with the accessible Q-ε ranges under the experimental conditions of this experiment. Filled diamonds correspond to the position of the inelastic peaks, the solid lines to the $Q(\varepsilon)$ relation for the specific detector settings at different scattering angles Θ. The tick marks refer to Bragg reflections of β-AgCuS.

measured at different angles results from coherent scattering, which was taken into account in the calculation of $G(\varepsilon)$ by averaging of the spectra. Two partially merged but well distinguished peaks at $\sim$ 6 and 10.5 meV are discernible in $G(\Theta, \varepsilon)$ measured with almost all detectors. The lowest-energy peak observed in $S(\Theta, \varepsilon)$ at $\varepsilon \sim 2.6$ meV is hardly visible in $G(\Theta, \varepsilon)$. The presence of a peak at $\varepsilon \sim 2.6$ meV in $G(\Theta, \varepsilon)$ of β-AgCuS is only indicated by a minor bending at the spectra recorded at $\Theta = 47.6$, 76.1, 80.9, 85.8, 90.7, 119.1 degrees. The phase transition into the superionic α-phase results in a change of the peaks at $\varepsilon \sim 6$ and 10.5 meV into one broad excitation region centered at $\sim$ 11 meV at 398 K (see figure 6.7). The energy transfer of inelastic modes, observed in the $S(\Theta, \varepsilon)$ and $G(\Theta, \varepsilon)$ spectra of β-AgCuS, are shown in figure 6.8 together with the kinematic curves corresponding to the detectors at different scattering angles. No such inelastic peaks were observed in α-AgCuS. As it can be seen from the dashed lines in figure 6.8, the modes at $\sim$ 2.6, 6, and 10.5 meV show almost dispersionless behavior $\neq f(Q)$.

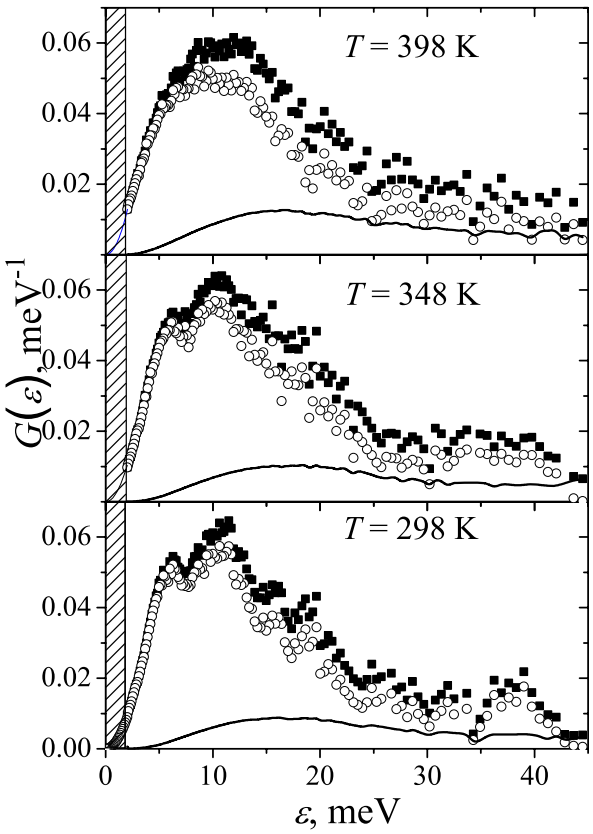

Figure 6.9: The phonon density of states in AgCuS at 298, 348 and 398 K; empty symbols - one-phonon scattering, thin lines - multiphonon scattering, filled symbols - total contribution. The dashed region corresponds to the energy range, where $G(\varepsilon)$ was extrapolated to 0 according to the Debye law.

6.2.2 Generalized neutron-weighted densities of states in β- and α-AgCuS

Generalized neutron-weighted densities of states in β- and α- AgCuS at 298, 348 and 398 K with calculated multiphonon and one-phonon contributions are shown in figure 6.9. The low-energy region ($\varepsilon < 2$ meV), where $G(\varepsilon)$ could not be analyzed because of the overlap with the elastic peak, is shown by hatching. The low energy part of $G(\varepsilon)$ demonstrates the linear dependence on ε, instead of the parabolic one $G(\varepsilon) \sim \varepsilon^2$ typical for 3D solids. We can assume that the linear dependence of $G(\varepsilon) \sim \varepsilon$ is connected with the presence of a low-energy mode. Temperature effects on generalized neutron-weighted densities of states in AgCuS have the same origin as in the case of AgCuSe and, therefore, will not be discussed in more detail.

Chapter 7

Summary

The temperature thresholds ($\approx$ 600 K) for the oxidation of $Cu_{2-\delta}Se$ during heating in air were determined by STA measurements for δ=0, 0.15, 0.25. On the other hand, a significant evaporation of selenium from the samples was observed in the TG curves, even in inert (Ar) atmosphere. The temperature thresholds for the decomposition of AgCuSe and AgCuS during heating in air are 600 and 570 K, respectively. In contrast to $Cu_{2-\delta}Se$, STA and diffraction measurements revealed that AgCuSe, AgCuS and Ag_3CuS_2 are stable in inert argon atmosphere even at high temperatures up to the melting points (1048, 936 and 998 K, respectively).

The discontinuous volume changes of about 1.4% [28] at the $\alpha \longrightarrow \beta$ superionic phase transition in Cu_2Se, 5% at the $\beta \longrightarrow \alpha$ transition in AgCuSe, 2.3% and 0.6% at the $\beta \longrightarrow \alpha$ and $\alpha \longrightarrow \delta$ transformations, respectively, in AgCuS as well as 0.77% and 0.58% at the $\beta \longrightarrow \alpha$ and $\alpha \longrightarrow \delta$ superionic phase transformations in Ag_3CuS_2 were revealed. Such large discontinuous volume changes are a proof of type I superionic transitions according to the classification of Boyce and Huberman [9], *i.e.*, all these compounds exhibit an abrupt transition into the highly conducting state. However, additional investigations are necessary to reveal the manner in which the superionic state in $Cu_{1.75}Se$ and $Cu_{1.85}Se$ is achieved.

The high-temperature phase sequences of stromeyerite ($\beta \overset{361K}{\longleftrightarrow} \alpha \overset{399K}{\longleftrightarrow} \alpha$ plus $\delta \overset{439K}{\longleftrightarrow} \delta$) and jalpaite ($\beta \overset{387K}{\longleftrightarrow} \alpha \overset{483K}{\longleftrightarrow} \alpha$ plus $\delta \overset{549K}{\longleftrightarrow} \delta$) are emphasized. The hcp arrangement of sulphur in both non-superionic β- and superionic α-AgCuS implies that the $\beta \longrightarrow \alpha$ transformation is due to cation disorder, whereas a rearrangement of the rigid anion sublattice

from hcp to fcc accompanies the $\alpha \longrightarrow \delta$ transformation. Hence, the superionic $\beta \longrightarrow \alpha$ and $\alpha \longrightarrow \delta$ transitions in stromeyerite have different origin. A similar situation occurs for the superionic transformations in jalpaite: β- and α-Ag_3CuS_2 adopt a distorted bcc sulphur sublattice, whereas a rearrangement of the bcc sulphur sublattice to fcc accompanies the $\alpha \longrightarrow \delta$ superionic transition. According to [90], there are only a few examples of structural phase transitions between two superionic phases accompanied by a rearrangement of the rigid anion sublattice. In the case of such a transition in stromeyerite (hcp$\longrightarrow$fcc) or jalpaite (bcc$\longrightarrow$fcc), investigations of the influence of different types of rigid anion sublattices on the ionic conductivity could elucidate the relationship between superionic conductivity and underlying crystal structure (see, for instance, a molecular dynamics modelling of the fcc$\longrightarrow$bcc transition in Ag_2Te [115] and bcc$\longrightarrow$fcc in Ag_2S [116]).

Detailed synchrotron and neutron powder diffraction studies revealed a common model for the time and spatial averaged distribution of the mobile cations in superionic β-$Cu_{2-\delta}Se$ with $\delta = 0$, 0.15 and 0.25 [57,60,64], α-AgCuSe [48,61] and δ-AgCuS [58,63] within a "defect" antifluorite structure. This model demonstrates a considerable degree of cation disorder in $\langle 111 \rangle$ directions, which can be modelled by a random occupation of the tetrahedral 8(c) site at $(\frac{1}{4}, \frac{1}{4}, \frac{1}{4})$ and the octahedral 32(f) site at (x, x, x) with $\frac{1}{3} < x < \frac{1}{2}$. Despite of the significant octahedral occupation there is minimum cation density on the ideal octahedral site 4(b) at $(\frac{1}{2}, \frac{1}{2}, \frac{1}{2})$. In the light of these crystal structure features, a model for ionic conduction in β-$Cu_{2-\delta}Se$ with δ=0, 0.15 and 0.25, α-AgCuSe and δ-AgCuS was derived from synchrotron and neutron powder diffraction: cations jump in skewed $\langle 100 \rangle$ directions between nearest-neighbour tetrahedral sites *via* the peripheries of the octahedral cavities. Furthermore, the temperature dependence of the cation distribution in α-AgCuSe as described in this model correlates well with the temperature behaviour of ionic conductivity and, hereby, gives strong support for the validity of the model [48]. The same correlation was revealed for δ-AgCuS [58]. On the other hand, the copper density near the boundary of the octahedral and tetrahedral voids, *i.e.* on the 32(f) site, increases with temperature and with the total copper content in β-$Cu_{2-\delta}Se$. With the assumption that the occupancy of the 32(f) site is the limiting factor for copper diffusion, a possible explanation of the decrease of ionic conductivity with increasing δ is given [57]. This is the main progress of the presented and

revised model for the cation distribution in β-$Cu_{2-\delta}Se$. Furthermore, the temperature and composition dependences of the distribution of copper ions between different interstitial sites might the reason for the different structure models proposed in literature for β-$Cu_{2-\delta}Se$. They can only be distinguished in a comprehensive study with complementary methods applied.

The high-temperature structural behaviour and a model for ionic conduction in hexagonal α-AgCuS were derived from synchrotron powder diffraction as well [58]. Similar to Cu_2S [91] the cation conductivity in α-AgCuS is 2-dimensional and occurs in slabs perpendicular to the c-direction. The principal common feature of α- and δ-AgCuS is that no evidence for cation jumps through $(\frac{1}{2}, \frac{1}{2}, \frac{1}{2})$ sites in $\langle 111 \rangle$ direction exists.

Single crystal studies of superionic β-Cu_2Se, α-AgCuSe, α- and δ-AgCuS as well as α- and δ-Ag_3CuS_2 could provide more information about the underlying structure. Such measurements are, however, practically impossible (or at least extremely difficult) even if single crystals are available, since the 1st order superionic phase transition will lead to fracture. In preliminary tests, all single crystals with well developed faces gave only very poor diffraction patterns with anomalous spot shapes.

Inelastic neutron scattering on non-superionic β-AgCuS revealed dispersionless modes in the low-energy part of the $S(\Theta, \varepsilon)$ and $G(\Theta, \varepsilon)$ spectra near 2.6, 6, and 10.5 meV. The existence of low-energy peaks at 2.6 meV agrees with results in literature for several superionics. The proposed correlation between the energy of the low-lying excitation and the mass of the heaviest ion of the superionic compound was confirmed. However, an additional experiment with better energy resolution is necessary to clarify the existence or absence of an excitation at $\sim$2 meV in the dynamic structure factor of non-superionic β-AgCuSe. The most interesting feature of the dynamic structure factor of superionic AgCuSe and AgCuS is the appearance of quasi-elastic scattering which corresponds to ionic motion through the structure.

The neutron-weighted density of states show a non-Debye-like behaviour for AgCuSe and AgCuS in the low-energy region accessed in INS experiments. In the light of the considerable anharmonicity of lattice vibrations, the harmonic approximation is not appropriate for a calculation of thermal properties. Pronounced changes with temperature in the frequency

spectra of β- and α-AgCuSe and β- and α-AgCuS result from numerous contributions (increasing anharmonic effects, time-averaged static disorder and phonon-phonon coupling) and accompany the superionic phase transitions. In principle, a separation of different contributions to the phonon widths is possible by inelastic coherent neutron scattering on single crystals (see for instance, [112]), but is practically impossible in the case of AgCuSe and AgCuS. Moreover, as can be seen in [117], molecular dynamics simulations are one of the most appropriate methods for the investigation of highly anharmonic solids. However, it is still a central problem for such simulations to derive a realistic potential, which reproduces the experimentally determined density of states within acceptable limits [117]. The proposed experimental results on the density of states in AgCuSe and AgCuS could be an experimental base for further computational modelling on this highly anharmonic system.

Finally, experimental studies by total (Bragg and diffuse) scattering on powdered samples or molecular dynamics simulations of diffusion pathways would provide further information about ionic transport in superionic systems.

Bibliography

[1] S. Hull. Superionics: crystal structures and conduction processes. *Rep. Prog. Phys.*, 67:1233–1314, 2004.

[2] D.A. Keen. Disordering phenomena in superionic conductors. *J. Phys.: Condens. Matter.*, 14:R819–R857, 2002.

[3] P.G. Bruce. Solid-state chemistry of lithium power sources. *Chem. Comm.*, pages 1817–1824, 1997.

[4] J.M. Tarascon and M. Armand. Issues and challenges facing rechargeable lithium batteries. *Nature*, 414:359–367, 2001.

[5] N. Bonanos, K.S. Knight, and B. Ellis. Perovskite solid electrolytes - structure, transport properties and fuel cell applications. *Solid State Ionics*, 79:161–170, 1995.

[6] L. Carrette, K.A. Friedrich, and U. Stimming. Fuel cells: principles, types, fuels, and applications. *Chem. Phys. Chem.*, 1:162–193, 2000.

[7] J.W. Fergus. The application of solid fluoride electrolytes in chemical sensors. *Sensors Actuators B*, 42:119–130, 1997.

[8] N. Imanaka and G. Adachi. Rare earth contribution in solid state electrolytes, especially in the chemical sensor field. *J. Alloy. Compd.*, 250:492–500, 1997.

[9] J. B. Boyce and B. A. Huberman. Superionic conductors - transitions, structures, dynamics. *Phys. Rep.*, 51:189–265, 1979.

[10] T. Ishikawa and S. Miyatani. Electronic and ionic conduction in $Cu_{2-\delta}Se$, $Cu_{2-\delta}S$ and $Cu_{2-\delta}$(Se, S). *J. Phys. Soc. Jpn.*, 42:159–167, 1977.

[11] R. A. Yakshibaev, V. N. Konev, and M. Kh. Balapanov. Ionic conductivity and diffusion in superionic conductor α-$Cu_{2-\delta}Se$. *Fizika Tverdogo Tela*, 26:3641–3645, 1984.

[12] S. Miyatani. Electronic and ionic conduction in $(Ag_xCu_{1-x})_2Se$. *J. Phys. Soc. Jpn.*, 34:423–432, 1973.

[13] S. Miyatani, Y. Miura, and H. Ando. Mixed conduction in AgCuSe. *J. Phys. Soc. Jpn.*, 46:1825–1832, 1979.

[14] M. Kh. Balapanov, R. A. Yakshibaev, and U. Kh. Muhamedyanov. Ion transfer in solid solutions of Cu_2Se and Ag_2Se superionic conductors. *Physics of the solid state*, 45:634–638, 2003.

[15] R. F. Kadrgulov, R. A. Yakshibaev, and M. A. Khasanov. Phase relations, ionic transport and diffusion in the alloys of Cu_2S-Ag_2S mixed conductors. *Ionics*, 7:156–160, 2001.

[16] A. Tonejc. Phase diagram and some properties of $Cu_{2-x}Se$ ($2.01 \geq 2\text{-}x \geq 1.75$). *J. Mater. Sci.*, 15:3090–3094, 1980.

[17] K. Yamamoto and S. Kashida. X-ray study of the average structure of Cu_2Se and $Cu_{1.8}S$ in the room-temperature and high-temperature phases. *J. Solid State Chem.*, 93:202–211, 1991.

[18] S. Kashida and J. Akai. X-ray diffraction and electron microscopy studies of the room-temperature structure of Cu_2Se. *J. Phys. C Solid State*, 21:5329–5336, 1988.

[19] J. Gladic, O. Milat, Z. Vucic, and V. Horvatic. Structural variants in the low-temperature β-phase of stoichiometric cuprous selenide. *J. Solid State Chem.*, 91:213–224, 1991.

[20] P. Rahlfs. Ueber die kubischen Hochtemperaturmodifikationen der Sulfide, Selenide und Telluride des Silbers und des einwertigen Kupfers. *Z. Phys. Chem.*, 31:157–194, 1936.

[21] W. Borchert. Gitterumwandlungen im System $Cu_{2-x}Se$. *Z. Kristallogr.*, 106:5–24, 1945.

[22] R. D. Heyding. Copper/selenium system. *Can. J. Chemistry*, 44:1233–1236, 1966.

[23] Z. Ogorelec and B. Celustka. On the relation between electrical conductivity and phase transition of non-stoichiometric cuprous selenides. *J. Phys. Chem. Solids*, 30:149–155, 1969.

[24] A. L. N. Stevels and F. Jellinek. Phase transitions in copper chalcogenides. *RECUEIL*, 111:273–283, 1971.

[25] Z. Ogorelec, B. Mestnik, and D. Devcic. A new contribution to the equilibrium diagram of the Cu-Se system. *J. Mater. Sci.*, 7:967–969, 1972.

[26] R. M. Murray and R. D. Heyding. The copper-selenium system at temperatures to 850 K and pressures to 50 kbar. *Can. J. Chemistry*, 53:878–886, 1975.

[27] A. Tonejc, Z. Ogorelec, and B. Mestnik. X-ray investigation of copper selenides $Cu_{2-x}Se$ ($2.00 \geq 2\text{-}x \geq 1.72$). *J. Appl. Crystallogr.*, 8:375–379, 1975.

[28] Z. Vucic, O. Milat, V. Horvatic, and Z. Ogorelec. Composition induced phase-transition splitting in cuprous selenide. *Phys. Rev. B*, 24:5398–5401, 1981.

[29] N. K. Abrikosov, V. F. Bankina, M. A. Korzhuev, G. K. Demenskii, and O. A. Teplov. Calorimetric study of superionic phase transition in $Cu_{2-x}Se$. *Fizika Tverdogo Tela*, 25:2911–2916, 1983.

[30] Z. Vucic, V. Horvatic, and O. Milat. Dilatometric study of nonstoichiometric copper selenide $Cu_{2-x}Se$. *Solid State Ionics*, 13:127–133, 1984.

[31] T. Ohtani, Y. Tachibana, J. Ogura, T. Miyake, Y. Okada, and Y. Yokota. Physical properties and phase transitions of β-$Cu_{2-x}Se$ ($0.20 \leq x \leq 0.25$). *J. Alloy. Compd.*, 279:135–141, 1998.

[32] A. Boettcher, G. Haase, and H. Treupel. Untersuchungen über die Strukturen und die Strukturumwandlungen der Sulfide und Selenide des Silbers und des Kupfers. *Z. Angew. Physik*, 10:478–487, 1955.

[33] N. Marimoto and M. Uchimizu. *X-ray powder data file 19 - 401.* Special Technical publications 480G ASTM, Philadelphia, 1969.

[34] A. L. N. Stevels. Phase transitions in nickel and copper selenides and tellurides. *Philips Res. Repts. Suppl.*, 9:1–124, 1969.

[35] O. Milat, Z. Vucic, and B. Ruscic. Superstructural ordering in low-temperature phase of superionic Cu_2Se. *Solid State Ionics*, 23:37–47, 1987.

[36] S. A. Danilkin, A. N. Skomorokhov, A. Hoser, H. Fuess, V. Rajevac, and N. N. Bickulova. Crystal structure and lattice dynamics of superionic copper selenide $Cu_{2-\delta}Se$. *J. Alloy. Compd.*, 361:57–61, 2003.

[37] K. D. Machado, J. C. de Lima, T. A. Grandi, C. E. M. Campos, C. E. Maurmann, A. A. M. Gasperini, S. M. Souza, and A. F. Pimenta. Structural study of $Cu_{2-x}Se$ alloys produced by mechanical alloying. *Acta Crystallogr. B*, 60:282–286, 2004.

[38] M. Oliveria, R. K. McMullan, and B. J. Wuensch. Single crystal neutron diffraction analysis of the cation distribution in the high-temperature phases α-$Cu_{2-x}S$, α-$Cu_{2-x}Se$ and α-Ag_2Se. *Solid State Ionics*, 28-30:1332–1337, 1988.

[39] K. Yamamoto and S. Kashida. X-ray study of the cation distribution in Cu_2Se, $Cu_{1.8}Se$ and $Cu_{1.8}S$; analysis by the maximum entropy method. *Solid State Ionics*, 48:241–248, 1991.

[40] R. D. Heyding and R. M. Murray. The crystal structures of $Cu_{1.8}Se$, Cu_3Se_2, α- and γ-CuSe, $CuSe_2$, and $CuSe_2$II. *Can. J. Chemistry*, 54:841–848, 1976.

[41] J. W. Earley. Description and synthesis of the selenide minerals. *Am. Mineral.*, 5:337–364, 1950.

[42] A. J. Frueh jr., G. K. Czamanske, and Ch. Knight. The crystallography of eucairite, CuAgSe. *Z. Kristallogr.*, 108:389–396, 1957.

[43] I. R. Nuriev, F. I. Aliev, and R. B. Shafi-Zade. Electron-diffraction investigation of Ag_2Se-Cu_2Se system. *Izvestiya akkademii nauk Azeibarzhanskoi SSR (in russian)*, 2:66–68, 1977.

[44] Sh. K. Kyazimov, G. Sh. Gasanov, and Yu. G. Asadov. Structural transitions in AgCuSe. *Doklady akademii nauk Azeibarzhanskoi SSR (in russian)*, 11:33–36, 1986.

[45] Sh. K. Kiazimov, K. M. Jafarov, and Yu. G. Asadov. Structural phase transitions in (Ag, Cu) S, Se, Te crystals. *Phase Transit.*, 21:11–21, 1990.

[46] T. Ohtani, K. Maruyama, and K. Ohshima. Synthesis of copper, silver, and samarium chalcogenides by mechanical alloying. *Mater. Res. Bull.*, 32:343–350, 1997.

[47] K. Chrissafis, N. Vouroutzis, K. M. Paraskevopoulos, N. Frangis, and C. Manolikas. Phase transformation in CuAgSe: a DSC and electron diffraction examination. *J. Alloy. Compd.*, 385:169–172, 2004.

[48] D. M. Trots, A. N. Skomorokhov, M. Knapp, and H. Fuess. High-temperature behaviour of average structure and vibrational density of states in the ternary superionic compound AgCuSe. *Eur. Phys. J. B*, 51:507–512, 2006.

[49] T. Shimoyama, M. Arai, and T. Sakuma. Crystal structure of superionic phase of CuAgSe. *1st international meeting on Superionic conductor physics, Kyoto*, 2003.

[50] C. L. Baker, F. J. Lincoln, and A. W. S. Johnson. A low-temperature structural phase transformation in CuAgS. *Acta Crystallogr.*, 47:891–899, 1991.

[51] C. Skarda, B. J. Wuensch, and E. Prince. Neutron powder diffraction study of the fast-ion conductor CuAgS between 20^o and 115^oC. *NBS Tech. Note*, 1160:57–63, 1981.

[52] N. Suhr. Concerning the Ag_2S-Cu_2S system. *Econ. Geol.*, 50:347–350, 1955.

[53] A. J. Frueh. The crystal structure of stromeyerite, AgCuS: a possible defect structure. *Z. Kristallogr.*, 106:299–307, 1955.

[54] S. Djurle. An X-ray study on the system Ag-Cu-S. *Acta Chem. Scand.*, 12:1427–1436, 1958.

[55] B. J. Skinner. The system Cu-Ag-S. *Econ. Geol.*, 61:1–26, 1966.

[56] C. L. Baker, F. J. Lincoln, and A. W. S. Johnson. Crystal structure determination of Ag_3CuS_2 from powder X-ray diffraction data. *Aust. J. Chem.*, 45:1441–1449, 1992.

[57] A. N. Skomorokhov, D. M. Trots, M. Knapp, N. N. Bickulova, and H. Fuess. Structural behaviour of β-$Cu_{2-\delta}Se$ (δ=0, 0.15, 0.25) in dependence of temperature studied by synchrotron powder diffraction. *J. Alloy. Compd.*, 421:64–71, 2006.

[58] D. M. Trots, A. Senyshyn, D. A. Mikhailova, M. Knapp, C. Baehtz, M. Hoelzel, and H. Fuess. High-temperature thermal expansion and structural behaviour of stromeyerite, AgCuS. *J. Phys.: Condens. Mat.*, 19:136204, 2007.

[59] A. N. Skomorokhov, D. M. Trots, S. G. Ovchinnikov, and H. Fuess. Lattice vibrations in an β- and α-AgCuS superionic conductor: experimental time-of-flight inelastic neutron scattering studies. *J. Phys.: Condens. Mat.*, 19:186228, 2007.

[60] D. Trots, M. Knapp, A. Skomorokhov, and H. Fuess. Structural behaviour of $Cu_{2-x}Se$ at high temperatures. *Hasylab annual report*, 1:361–362, 2004.

[61] D. Trots, M. Knapp, and H. Fuess. High-temperature synchrotron diffraction on the ternary superionic compound AgCuSe. *Hasylab annual report*, 1:363–364, 2005.

[62] D. M. Trots, D. A. Mikhailova, and H. Fuess. High-temperature phase transitions and thermal expansion of jalpaite, Ag_3CuS_2. *Hasylab annual report*, 1:547–545, 2006.

[63] D. M. Trots, C. Baehtz, and H. Fuess. High-temperature phase transitions and thermal expansion of stromeyerite, AgCuS. *Hasylab annual report*, 1:549–550, 2006.

[64] A. Skomorokhov, M. Knapp, V. Rajevac, and H. Fuess. X-ray diffraction study of the high-temperature structure of $Cu_{2-\delta}Se$. *Hasylab annual report*, 1:595–596, 2002.

[65] M. Knapp, C. Baehtz, H. Ehrenberg, and H. Fuess. The synchrotron powder diffractometer at beamline B2 at Hasylab/DESY: status and capabilities. *J. Synchrotron radiat.*, 11:328–334, 2004.

[66] M. Knapp, V. Joco, C. Baehtz, H.H. Brecht, A. Berghaeuser, H. Ehrenberg, H. von Seggern, and H. Fuess. Position-sensitive detector system OBI for high resolution X-ray powder diffraction using on-site readable image plates. *Nucl. Instrum. Meth. A*, 521:565–570, 2004.

[67] M. Hoelzel, A. Senyshyn, R. Gilles, H. Boysen, and H. Fuess. The structure powder diffractometer Spodi at the FRM II. *Neutron News*, submitted.

[68] http://www-llb.cea.fr/fullweb/powder.htm.

[69] A. Le Bail, H. Duroy, and J. L. Fourquet. Ab-initio structure determination of $LiSbWO_6$ by X-ray powder diffraction. *Mater. Res. Bull.*, 23:447–452, 1988.

[70] L. B. McCusker, R. B. Von Dreele, D. E. Cox, D. Louer, and P. Scardi. Rietveld refinement guidelines. *J. Appl. Crystallogr.*, 32:36–50, 1999.

[71] R. A. Young, editor. *The Rietveld Method*. Oxford University Press, 1993.

[72] P. Karen and P. M. Woodward. Liquid-mix disorder in crystalline solids: $ScMnO_3$. *J. Solid. State Chem.*, 141:78–88, 1998.

[73] http://www.ncnr.nist.gov/programs/crystallography/software/cmpr/.

[74] Yu. V. Taran. *User Guide. Neutron Experimental Facilities at JINR (Dubna: JINR Press).*, 1992.

[75] http://www.cacr.caltech.edu/projects/danse/arcsbook16x.pdf.

[76] S. G. Ovchinnikov and A. N. Skomorokhov. Data reduction package at DIN-2PI. *Vestnik Fiziko-Energeticheskogo Instituta (FEI bulletin)*, to be published.

[77] E.J. Lindley and J. Mayers. *Experimental Method and Correction to Data, in: Neutron Scattering at a Pulsed Source*. Bristol and Philadelphia, 1988.

[78] V. S. Oskoskii. Measurement of phonon distribution function in polycrystalline materials using coherent scattering of slow neutrons into a solid angle. *Sov. Phys.-Solid State*, 9:420–422, 1967.

[79] J. Wuttke, M. Kiebel, E. Bartsch, F. Fujara, W. Petry, and H. Sillescu. Relaxation and phonons in viscous and glassy orthoterphenyl. *Z. Phys. B Cond. Mat.*, 91:357–365, 1993.

[80] J. Dawidowski, F. J. Bermejo, and J. R. Granada. Efficient procedure for the evaluation of the multiple scattering and multiphonon corrections in inelastic neutron-scattering experiments. *Phys. Rev. B*, 58:706–715, 1998.

[81] O. Kubaschewski and B.E. Hopkins. *Oxidation of Metals and Alloys.* second ed., Butterworth, London, 1962.

[82] M. Komatsu and H. Mori. In situ HVEM study on copper oxidation using an improved environmental cell. *J. Electron. Microsc.*, 54:99–107, 2005.

[83] V.L. Barone, I.L. Botto, and I.B. Schalamuk. Thermal effects of minority chalcogenide minerals: DTA-TG, IR spectroscopy and SEM electron microscopy studies. *Lat. Am. Appl. Res.*, 33:1–6, 2003.

[84] W. Buehrer, F. Altorfer, J. Mesot, H. Bill, P. Carron, and H. G. Smith. Lattice dynamics and the diffuse phase transition of lithium sulphide investigated by coherent neutron scattering. *J. Phys.: Condens. Mat.*, 3:1055–1064, 1991.

[85] P. Scardi, M. Leoni, and R. Delhez. Line broadening analysis using integral breadth methods: a critical review. *J. Appl. Crystallogr.*, 37:381–390, 2004.

[86] D. A. Keen and S. Hull. Determination of structural disorder in superionic Ag_2Te by neutron total scattering. *J. Phys.: Condens. Matter.*, 10:8217–8234, 1998.

[87] D. A. Keen and S. Hull. The high-temperature structural behaviour of copper(I) iodide. *J. Phys.: Condens. Matter.*, 7:5793–5804, 1995.

[88] S. Hull, D. A. Keen, and P. Berastegui. Structural description of superionic behaviour in the system $(AgI)_x$–$(PbI_2)_{1-x}$, $\frac{2}{3} \leq x \leq \frac{4}{5}$. *Solid State Ionics*, 147:97–106, 2002.

[89] D. A. Keen, S. Hull, A. C. Barnes, P. Berastegui, W. A. Crichton, P. A. Madden, M. G. Tucker, and M. Wilson. Nature of the superionic transition in Ag^+ and Cu^+ halides. *Phys. Rev. B*, 68:014117, 2003.

[90] S. Hull and D. A. Keen. Structural characterization of further high temperature superionic phases of Ag_2HgI_4 and Cu_2HgI_4. *J. Phys.: Condens. Mat.*, 13:5597–5610, 2001.

[91] R. J. Cava, F. Reidinger, and B. J. Wuensch. Mobile ion distribution and anharmonic thermal motion in fast ion conducting Cu_2S. *Solid State Ionics*, 5:501–504, 1981.

[92] A. Yoshiasa, A. Inaba, T. Ishii, and K. Koto. A phase transition of AgI at 150 K. *Solid State Ionics*, 79:67–70, 1995.

[93] D. A. Keen and S. Hull. Determination of the structure of β-CuI by high-resolution neutron powder diffraction. *J. Phys.: Condens. Mat.*, 6:1637–1644, 1994.

[94] K. A. Schönau and S. A. T. Redfern. High-temperature phase transitions, dielectric relaxation, and ionic mobility of proustite, Ag_3AsS_3, and pyrargyrite, Ag_3SbS_3. *J. Appl. Phys.*, 92:7415–7424, 2002.

[95] S. Hull and D. A. Keen. Structural characterization of the $\beta \longrightarrow \alpha$ superionic transition in Ag_2HgI_4 and Cu_2HgI_4. *J. Phys.: Condens. Mat.*, 12:3751–3765, 2000.

[96] T. Ishii. Cluster-induced local distortion in ionic conductors – negative static expansion. *Solid State Commun.*, 108:513–517, 1998.

[97] T. Ishii and O. Kamishima. Cluster-induced local distortions and superionic transitions of ionic conductors AgI and PbF_2. *J. Phys. Soc. Jpn.*, 70:159–166, 2001.

[98] T. Seko and T. Ishii. MD investigation of defect-induced negative expansion of c-axis in β-AgI. *J. Phys. Soc. Jpn.*, 67:1837–1839, 1998.

[99] T. Sakuma and K. Shibata. Low-energy excitation in β-Cu_2Se. *J. Phys. Soc. Jpn.*, 58:3061–3064, 1989.

[100] T. Sakuma, K. Shibata, and S. Hoshino. Low-energy excitation in CuI. *Solid State Ionics*, 53-56:1278–1281, 1992.

[101] T. Sakuma, M. Mutou, K. Ohki, M. Arai, H. Takahashi, and Y. Ishii. Low-energy excitation in $CsPbX_3$ (X =Cl, Br). *Solid State Ionics*, 154-155:237–242, 2002.

[102] H. Takahashi, Y. Hiki, T. Sakuma, and S. Funahashi. Inelastic neutron scattering of $(AgI)_x(AgPO_3)_{1-x}$ glasses. *Solid State Ionics*, 53-56:1164–1167, 1992.

[103] W. Buhrer, R. M. Nicklow, and P. Bruesch. Lattice dynamics of β-(silver iodide) by neutron scattering. *Phys. Rev. B*, 17:3362–3370, 1978.

[104] K. Funke. Quasielastic and inelastic scattering of cold neutrons from silver iodide. *Solid State Commun.*, 14:1021–1024, 1974.

[105] K. Wakamura. Roles of phonon amplitude and low-energy optical phonons on superionic conduction. *Phys. Rev. B*, 56:11593–11599, 1997.

[106] K. Wakamura. Origin of the low-energy mode in superionic conductors. *Phys. Rev. B*, 59:3560–3568, 1999.

[107] L. L. Boyer. Nature of melting and superionicity in alkali and alkaline-earth halides. *Phys. Rev. Lett.*, 45:1858–1862, 1980.

[108] L. L. Boyer. Origin of superionicity in the alkaline earth halides. *Solid State Ionics*, 5:581–584, 1981.

[109] K. Wakamura. Interpretation of high ionic conduction in superionic conductors based on electronic and phonon properties. *Solid State Ionics*, 171:229–235, 2004.

[110] G. Eckold, K. Funke, J. Kalus, and R. E. Lechner. The diffusive motion of silver ions in α-AgI: Results from quasielastic neutron scattering. *J. Phys. Chem. Solids*, 37:1097–1103, 1976.

[111] M. A. Hamilton, A. C. Barnes, W. S. Howells, and H. E. Fischer. Ag^+ dynamics in the superionic and liquid phases of Ag_2Se and Ag_2Te by coherent quasi-elastic neutron scattering. *J. Phys.: Condens. Mat.*, 13:2425–2436, 2001.

[112] M. B. Salamon. *Physics of Superionic Conductors*. Springer-Verlag, 1979.

[113] K. Schmalzl, D. Strauch, and H. Schober. Lattice-dynamical and ground-state properties of CaF_2 studied by inelastic neutron scattering and density-functional methods. *Phys. Rev. B*, 68:144301, 2003.

[114] P. D. Bogdanoff, B. Fultz, J. L. Robertson, and L. Crow. Temperature dependence of the phonon entropy of vanadium. *Phys. Rev. B*, 65:014303, 2001.

[115] F. Shimojo and H. Okazaki. Fcc-bcc phase transition of the Te sublattice in superionic conductor Ag_2Te: a molecular dynamics study. *J. Phys. Soc. Jpn.*, 61:4465–4473, 1992.

[116] S. Hull, D. A. Keen, D. S. Sivia, P. A. Madden, and M. Wilson. The high-temperature superionic behaviour of Ag_2S. *J. Phys.: Condens. Mat.*, 14:L9–L17, 2002.

[117] J. X. M. Zheng-Johansson, I. Ebbsjö, and R.L. McGreevy. A molecular dynamics study of ionic conduction in CuI. I. Derivation of the interionic potential from dynamic properties. *Solid State Ionics*, 82:115–122, 1995.

Appendix A

Tables of structural parameters

Table A.1: Structure parameters of β-$Cu_{1.75}Se$ in the temperature range 298-573 K. Powder diffraction data were collected with the B2 diffractometer. Space group $Fm\bar{3}m$; $Z = 4$; atom positions: Cu^{+} in 8(c) site at ($\frac{1}{4}$, $\frac{1}{4}$, $\frac{1}{4}$) and on 32(f) site at (x, x, x), Se^{-2} on 4(a) site at (0, 0, 0). Refined parameters: isotropic thermal displacement of anions u_{anion} and cations u_{cation}, cation positional parameters x, cation site occupancies on 8(c) and 32(f) sites; parameter constraints: isotropic thermal parameters of cations, sum of cation site occupancies.

Temperature (K)	a (Å)	V/Z (Å^3)	x	u_{anion} (Å^2)	u_{cation} (Å^2)	Occupancy of 32(f) sites (%)
298	5.7550(3)	47.651	0.386(6)	0.027(3)	0.036(3)	1.73(28)
323	5.7599(4)	47.773	0.391(5)	0.029(4)	0.034(4)	2.26(34)
348	5.7641(4)	47.878	0.387(5)	0.033(3)	0.038(4)	2.52(36)
373	5.7677(3)	47.968	0.385(4)	0.033(4)	0.040(2)	2.77(20)
398	5.7716(3)	48.065	0.378(4)	0.037(4)	0.041(3)	3.45(30)
423	5.7755(3)	48.162	0.376(4)	0.034(3)	0.047(4)	3.51(29)
448	5.7796(3)	48.265	0.380(3)	0.039(4)	0.048(4)	3.71(28)
473	5.7828(4)	48.345	0.376(2)	0.042(2)	0.049(3)	4.44(23)
498	5.7866(3)	48.441	0.340(2)	0.041(4)	0.054(3)	4.65(30)
523	5.7903(3)	48.534	0.370(5)	0.040(4)	0.064(4)	4.27(39)
548	5.7939(2)	48.624	0.375(2)	0.043(3)	0.070(3)	4.32(26)
573	5.7981(2)	48.730	0.375(3)	0.048(3)	0.068(4)	4.99(29)

Table A.2: As table A.1, but for β-$Cu_{1.85}Se$ in the temperature range 353-573 K.

Temperature (K)	a (Å)	V/Z (Å^3)	x	u_{anion} (Å^2)	u_{cation} (Å^2)	Occupancy of 32(f) sites (%)
353	5.7817(7)	48.318	0.353(1)	0.017(3)	0.041(5)	3.56(30)
373	5.7853(7)	48.408	0.358(1)	0.017(4)	0.044(7)	4.12(31)
393	5.7876(7)	48.466	0.349(1)	0.015(5)	0.046(8)	4.27(34)
413	5.7909(9)	48.549	0.363(1)	0.018(7)	0.060(6)	3.74(30)
433	5.7929(6)	48.599	0.364(1)	0.020(6)	0.061(7)	4.34(30)
453	5.7973(8)	48.710	0.375(1)	0.022(7)	0.067(5)	3.67(27)
473	5.7992(7)	48.758	0.373(1)	0.021(6)	0.066(7)	4.10(25)
493	5.8020(8)	48.828	0.376(1)	0.030(5)	0.072(5)	4.84(25)
513	5.8040(4)	48.879	0.373(1)	0.027(6)	0.068(7)	4.88(22)
533	5.8067(8)	48.947	0.376(1)	0.030(7)	0.070(5)	4.87(21)
553	5.8091(4)	49.008	0.370(1)	0.030(6)	0.071(6)	5.17(25)
573	5.8130(7)	49.107	0.368(1)	0.035(8)	0.076(7)	5.86(25)

Table A.3: As table A.1, but for β-Cu_2Se and β-$Cu_{1.95}Se$.

Temperature (K)	δ	a (Å)	V/Z (Å^3)	x	u_{anion} (Å^2)	u_{cation} (Å^2)	Occupancy of 32(f) sites (%)
423	0	5.8422(6)	49.850	0.390(2)	0.040(7)	0.049(7)	6.20(33)
553	0.05	5.8398(7)	49.789	0.388(2)	0.047(7)	0.055(7)	7.00(39)
563	0.05	5.8406(7)	49.809	0.397(2)	0.0518(5)	0.068(6)	7.59(40)
573	0.05	5.8417(7)	49.838	0.393(3)	0.051(7)	0.060(2)	6.73(35)

Table A.4: Thermal expansion of β-AgCuSe in the temperature range 300-473 K. Powder diffraction data were collected with B2 diffractometer and evaluated by structure independent (Le Bail) fit based on a large orthorhombic supercell $a\times10a'\times2c$ with Z=40 (space group $Pmmn$).

T (K)	a (Å)	a' (Å)	c (Å)	V/Z (Å^3)
300	4.1274(10)	4.0711(10)	6.3232(10)	53.125
323	4.13053(8)	4.07124(8)	6.32172(9)	53.154
373	4.13291(7)	4.07710(7)	6.32341(7)	53.276
423	4.13436(7)	4.08404(7)	6.32520(7)	53.400
473	4.12651(8)	4.13951(8)	6.31434(9)	53.930

Table A.5: As table A.1, but for α-AgCuSe in the temperature range 523-973 K.

Temperature (K)	a (Å)	V/Z (Å^3)	x	u_{anion} (Å^2)	u_{cation} (Å^2)	Occupancy of 32(f) sites (%)
523	6.1002(8)	56.752	0.419(2)	0.076(5)	0.158(6)	11.71(20)
573	6.1165(5)	57.208	0.416(2)	0.094(6)	0.193(6)	11.80(24)
623	6.1284(5)	57.5414	0.411(2)	0.091(6)	0.192(6)	12.06(25)
673	6.1375(7)	57.799	0.405(2)	0.100(9)	0.190(5)	12.17(25)
723	6.1500(8)	58.153	0.406(5)	0.104(6)	0.209(6)	12.12(30)
773	6.1567(7)	58.343	0.408(2)	0.110(6)	0.213(5)	11.92(14)
823	6.1655(7)	58.594	0.405(2)	0.100(8)	0.207(7)	12.47(34)
873	6.1742(8)	58.842	0.405(2)	0.099(9)	0.207(7)	12.44(34)
923	6.1849(6)	59.149	0.404(3)	0.112(10)	0.2506(8)	12.12(30)
973	6.1950(11)	59.437	0.410(5)	0.104(8)	0.269(11)	12.00(30)

Table A.6: Structure parameters of β-AgCuS in the temperature range 298-354 K. Powder diffraction data were collected with B2 diffractometer. Space group $Cmc2_1$, $Z = 4$.

T (K)	298	304	316	329	341	354
a (Å)	4.0633(2)	4.06349(11)	4.06428(12)	4.06460(14)	4.06555(15)	4.06685(13)
b (Å)	6.6281(4)	6.6289(2)	6.6304(2)	6.6316(3)	6.6335(3)	6.6361(3)
c (Å)	7.9713(4)	7.9719(2)	7.9722(2)	7.9698(3)	7.9679(3)	7.9667(3)
S, site	4(a)					
x	$\frac{1}{2}$					
y	0.287(2)	0.2820(5)	0.2826(5)	0.2811(6)	0.2818(6)	0.2807(6)
z	0.259(8)	0.264(2)	0.265(2)	0.267(2)	0.268(1)	0.261(2)
u_{iso} (Å^2)	0.020(2)	0.020(2)	0.020(1)	0.020(1)	0.020(2)	0.021(1)
Occupancy (%)	100					
Ag, site	4(a)					
x	$\frac{1}{2}$					
y	0.495					
z	$\frac{1}{2}$					
u_{iso} (Å^2)	0.0787(13)	0.0787(15)	0.0788(10)	0.0788(10)	0.0790(10)	0.080(1)
Occupancy (%)	100					
Cu, site	4(a)					
x	0					
y	0.432(1)	0.4329(3)	0.4339(3)	0.4321(3)	0.4321(3)	0.4330(3)
z	0.248(2)	0.244(2)	0.243(1)	0.243(1)	0.246(1)	0.242(1)
u_{iso} (Å^2)	0.0287(15)	0.0287(15)	0.029(1)	0.0287(15)	0.300(1)	0.301(1)
Occupancy (%)	100					

Table A.7: Structure parameters of α-AgCuS in the temperature range 367-432 K. Powder diffraction data were collected with B2 diffractometer. Space group $P6_3/mmc$, $Z = 2$. The isotropic thermal parameters u_{iso} of cations and copper occupancy in 2(b) and 12(k) positions were constrained during refinements. Positional parameters of silver and copper in 12(k) positions were constrained as well (at that $y = 2x$).

T (K)	367	380	393	406	419	432
a (Å)	4.137(1)	4.1434(5)	4.1519(5)	4.1524(5)	4.1485(5)	4.1448(6)
c (Å)	7.096(2)	7.0813(8)	7.0692(9)	7.0575(9)	7.0446(9)	7.0325(10)
$V_{fraction}$	1	1	1	0.99	0.95	0.8
S, site			2(d)			
x			$\frac{1}{3}$			
y			$\frac{2}{3}$			
z			$\frac{3}{4}$			
u_{iso} (Å^2)	0.090(12)	0.089(1)	0.070(11)	0.063(13)	0.063(14)	0.076(13)
Occupancy (%)			100			
Ag, site			12(k)			
x	0.247(3)	0.246(1)	0.250(1)	0.247(2)	0.254(2)	0.257(1)
y	0.495(6)	0.492(2)	0.500(2)	0.494(4)	0.508(4)	0.514(2)
z	0.437(2)	0.436(1)	0.431(1)	0.431(1)	0.431(1)	0.429(1)
u_{iso} (Å^2)	0.200(7)	0.200(8)	0.187(13)	0.182(19)	0.196(13)	0.177(13)
Occupancy (%)			16.7			
Cu, site			12(k)			
x	0.247(3)	0.246(1)	0.250(1)	0.247(2)	0.254(2)	0.257(1)
y	0.495(6)	0.492(2)	0.500(2)	0.494(4)	0.508(4)	0.514(2)
z	0.437(2)	0.436(1)	0.431(7)	0.432(8)	0.431(1)	0.429(1)
u_{iso} (Å^2)	0.200(7)	0.200(8)	0.187(13)	0.182(19)	0.196(13)	0.177(13)
Occupancy (%)	3.9(9)	4.1(8)	4.0(6)	4.1(8)	4.0(9)	4.2(9)
Cu, site			2(b)			
x			0			
y			0			
z			$\frac{1}{4}$			
u_{iso} (Å^2)	0.200(7)	0.200(8)	0.187(13)	0.182(19)	0.196(13)	0.177(13)
Occupancy (%)	76.6(9)	75.4(8)	76.2(6)	75.2(8)	75.8(9)	74.8(9)

Table A.8: As table A.1, but for δ-AgCuS in the temperature range 406-693 K.

Temperature (K)	$V_{fraction}$	a (Å)	V/Z (Å^3)	x	$u_{overall}$ (Å^2)	Occupancy of 32(f) sites (%)
406	0.01	5.9721(9)	53.251	0.3810(7)	0.146(13)	15.78(13)
419	0.05	5.9641(7)	53.036	0.3789(5)	0.139(7)	14.89(19)
432	0.20	5.9567(7)	52.838	0.3789(5)	0.139(7)	15.26(19)
446	1	5.9526(3)	52.730	0.3789(5)	0.144(7)	14.71(13)
460	1	5.9564(6)	52.830	0.3790(4)	0.144(7)	14.68(13)
473	1	5.9568(6)	52.841	0.3790(6)	0.155(10)	14.75(19)
487	1	5.9602(5)	52.932	0.3784(8)	0.155(13)	15.26(42)
501	1	5.9604(7)	52.938	0.3791(6)	0.166(10)	15.11(19)
515	1	5.9640(8)	53.035	0.3791(6)	0.174(12)	15.32(20)
529	1	5.9668(9)	53.108	0.3792(7)	0.161(12)	15.18(20)
543	1	5.9690(10)	53.167	0.379(1)	0.130(9)	14.89(18)
558	1	5.9723(7)	53.257	0.3789(6)	0.125(9)	15.08(18)
572	1	5.9741(6)	53.303	0.3772(7)	0.141(10)	15.06(20)
587	1	5.9771(7)	53.383	0.3785(7)	0.161(12)	15.41(22)
602	1	5.9788(10)	53.430	0.3775(5)	0.134(6)	14.96(13)
641	1	5.9863(10)	53.632	0.3804(11)	0.119(10)	13.34(24)
693	1	5.9917(10)	53.777	0.3800(8)	0.133(12)	14.39(24)

Table A.9: As table A.1, but for δ-AgCuS in the temperature range 460-890 K; powder diffraction data were collected with SPODI diffractometer.

Temperature (K)	a (Å)	V/Z (Å^3)	x	$u_{overall}$ (Å^2)	Occupancy of 32(f) sites (%)
460	5.954(1)	52.77	0.370(1)	0.149(10)	14.38(22)
478	5.958(1)	52.87	0.371(2)	0.159(13)	14.77(42)
640	5.986(1)	53.62	0.374(2)	0.190(13)	15.30(91)
785	6.010(1)	54.27	0.373(2)	0.158(13)	15.14(17)
890	6.027(1)	54.73	0.373(1)	0.183(12)	15.15(52)

Table A.10: Thermal expansion of Ag_3CuS_2 in the temperature range from RT up to the melting point. Powder diffraction data were collected with B2 diffractometer and evaluated by structure independent (Le Bail) fit.

β-Ag_3CuS_2, space group $I4_1/amd$				
Temperature (K)	a (Å)	c (Å)	c/a	V/Z (Å^3)
290	8.6503(3)	11.7858(4)	1.362	110.239
304	8.6551(2)	11.7825(2)	1.361	110.331
316	8.6626(2)	11.7738(2)	1.359	110.439
329	8.67001(15)	11.7652(2)	1.357	110.547
341	8.6772(2)	11.7561(2)	1.355	110.645
354	8.68508(15)	11.7445(2)	1.352	110.737
367	8.6936(2)	11.7321(3)	1.349	110.838
380	8.7066(2)	11.72091(25)	1.346	111.064
α-Ag_3CuS_2, space group $Im\overline{3}m$				
Temperature (K)	a_{bcc} (Å)	V_{bcc}/Z (Å^3)		
393	4.8177(2)	111.820		
406	4.8179(6)	111.834		
419	4.8198(5)	111.966		
432	4.8209(2)	112.043		
446	4.8230(3)	112.189		
459	4.8234(2)	112.217		
473	4.8239(2)	112.252		
α + δ-Ag_3CuS_2, $Im\overline{3}m$+$Fm\overline{3}m$				
Temperature (K)	a_{bcc} (Å)	V_{bcc}/Z (Å^3)	a_{fcc} (Å)	V_{fcc}/Z (Å^3)
487	4.8289(3)	112.602	6.0652(6)	111.559
501	4.8334(5)	112.917	6.0746(6)	112.079
515	4.8381(5)	113.246	6.0832(4)	112.555
543	4.8462(4)	113.816	6.0963(5)	113.284
δ-Ag_3CuS_2, space group $Fm\overline{3}m$				
Temperature (K)			a_{fcc} (Å)	V_{fcc}/Z (Å^3)
641			6.1143(6)	114.290
692			6.1230(4)	114.779
745			6.1254(4)	114.913
799			6.1398(4)	115.726
854			6.1478(4)	116.179
910			6.1571(5)	116.707
968			6.1674(6)	117.294

Acknowledgements

I am indebted to my scientific advisor Prof. Dr.-Ing. Dr. h. c. H. Fuess for the extremely interesting target setting, for his support and supervision.

I am very grateful to Dr. A. N. Skomorokhov from the Institute for Physics and Power Engineering, Obninsk, Russia, for his continuous interest and support throughout the last three years and for his help with the INS experiments.

I also would like to thank Dr. A. T. Senyshyn, Dr. G. B. Stryganyuk, Dr. M. Knapp, J. M. Engel, Dr. H. Ehrenberg, Dr. D. A. Mikhailova, Dr. V. Rajevac, Dr. K. G. Bramnik and Dr. N. N. Bramnik for their ardent support and a number of not merely powerful scientific but also comradely discussions.

Dr. V. Semenov (Institute for Physics and Power Engineering, Obninsk, Russia) and V. Morozov (Joint Institute for Nuclear research, Dubna, Russia) are gratefully acknowledged for their assistance with the INS measurements. I am indebted to C. Fasel for her help in the STA measurements and to Dr. P. Erhart for his help in the preparation of the manuscript of one of my publications.

Special thanks refers to my parents Myroslav and Nataliya, my wife Iryna, to my grandmothers Sofiya and Valentyna as well as my brothers Andrii and Valerii.

Finally, I would like thank to all colleagues from the Institute for Materials Science, TU Darmstadt.

This work was funded by the Bundesministerium für Bildung und Forschung, project number 03DU03D1 "Untersuchung von superionisch leitenden Kupferselenid-Legierungen mittels Neutronenstreuung" and by the Helmholtz Association of National Research Centers (grant number VH-VI 102).

Erklärung – Disclaimer

Die vorliegende Arbeit wurde im Zeitraum von Februar 2004 bis Februar 2007 im Fachgebiet Strukturforschung am Institut für Materialwissenschaft der Technischen Universität Darmstadt bei Herrn Prof. Dr.-Ing. Dr. h. c. H. Fuess angefertigt.

Hiermit erkläre an Eides Statt, dass ich meine Dissertation selbständig und nur mit den angegebenen Hilfsmitteln angefertigt habe und noch keinen Promotionsversuch unternommen habe.

Curriculum Vitae

Education:

• 5th Kovel school of general education, Ukraine (1986-1994).

• Kovel Machine-Building Technical School, Ukraine (1994-1998).

• MSc degree at Department of Semiconductor Electronics, Lviv Polytechnic National University, Ukraine (1998-2003).

• Institute for Materials Science, TU Darmstadt (2004-present).

Research Experience:

• 2002-2003 – research assistant at the Lviv Polytechnic National University including scientific visit at TU Darmstadt for one month supported by DAAD (Leonard - Euler Program).

• 2004-present – research scientist, PhD student at Strukturforschung, TU Darmstadt.

• March 2006 - present – beam-line scientist at the powder diffractometer B2 at Hasylab/DESY in Hamburg.

Personal Data:

• Date of birth: 17 March 1980.

• Place of birth: Kovel, Volyn region, Ukraine.

• Citizenship: Ukraine.

• Marital status: married.

• E-mail: d_trots@yahoo.com.

Publications based on the presented dissertation

• A. N. Skomorokhov, D. M. Trots, M. Knapp, N. N. Bickulova, H. Fuess. Structural behaviour of β-$Cu_{2-\delta}Se$ (δ = 0, 0.15, 0.25) in dependence on temperature studied by syn-

chrotron powder diffraction. *J. Alloy Compd.*, 412: 64-71, 2006.

• D. M. Trots, A. N. Skomorokhov, M. Knapp and H. Fuess. High-temperature behaviour of average structure and vibrational density of states in the ternary superionic compound AgCuSe. *Eur. Phys. J. B*, 51: 507-512, 2006.

• D. M. Trots, A. Senyshyn, D. A. Mikhailova, M. Knapp, C. Baehtz, M. Hoelzel and H. Fuess. High-temperature thermal expansion and structural behaviour of stromeyerite, AgCuS. *J. Phys.: Condens. Mat.*, 19: 136204, 2007.

• A. N. Skomorokhov, D. M. Trots, S. G. Ovchinnikov, H. Fuess. Lattice vibrations in an α- and β-AgCuS superionic conductor: experimental time-of-flight inelastic neutron scattering studies. *J. Phys.: Condens. Mat.*, 19: 186228, 2007.

Other publications

• D. I. Savytskii, D. M. Trots, L. O. Vasylechko, N. Tamura, M. Berkowski. Twinning in $La_{0.95}Sr_{0.05}Ga_{0.9}Mg_{0.1}O_{2.92}$ crystal studied by white-beam (Laue) X-ray microdiffraction. *J. Appl. Crystallogr.*, 36: 1197-1203, 2003.

• D. Savytskii, D. Trots, A. Matkovskii, C. Paulmann, U. Bismayer, M. Berkowski. Real structure of LSGMO crystal studied by Laue method. Mixed Ionic Electronic Conducting (MIEC) Perovskites for Advanced Energy Systems, NATO Science Series, Nina Orlovskaya, Nigel Browning, Kluwer Academic Publishers, Boston/Dordrecht/London, 173: 239-245, 2004.

• L. Vasylechko, A. Senyshyn, D. Trots, R. Niewa, W. Schnelle, M. Knapp. $CeAlO_3$ and $Ce_{1-x}R_xAlO_3$ (R = La, Nd) solid solutions: Crystal structure, thermal expansion and phase transitions. *J. Solid. State Chem.*, 180: 1277-1290, 2007